CHAPTER 8

Impact of mutations in the SARS-CoV-2 spike RBD region of Delta and Delta-Plus variants on its interaction with ACE2 Receptor Protein

Impact of mutations in the SARS-CoV-2 spike RBD region of Delta and Delta-Plus variants on its interaction with ACE2 Receptor Protein

8.1. Abstract:

The outbreak of severe acute respiratory syndrome coronavirus 2 (SARS CoV-2) has undergone multiple significant mutations since its detection in 2019 in Wuhan, China. The emergence of new SARS-CoV-2 variants that can spread rapidly and undermine vaccine-induced immunity threatens the end of the COVID-19 pandemic. The delta variant (B.1.617.2) emerged in India challenges efforts to control the COVID-19 pandemic. In addition to Delta, so called Delta Plus sub-variants (B.1.617.2.1 and B.1.617.2.2) have become a new cause of global concern. Here we compare the interaction profile of RBD of spike protein of the Delta and Delta-Plus variant of SARS-CoV-2 with ACE2 receptor. From the MD simulation, we observed the spike protein of Delta and Delta-Plus variant of SARS-CoV-2 utilises unique strategies to have stable binding with ACE2. Using MM-GBSA/MM-PBSA algorithms, we found the binding affinity of spike protein of the Delta- variant-ACE2 complex is indeed high (GB_{TOT} = -39.36 kcal/mol, PB_{TOT}= -17.52 kcal/mol) in comparison with spike protein of Delta-Plus variant-ACE2 Complex (GB_{TOT} = -36.83 kcal/mol, PB_{TOT} = -16.03 kcal/mol). Stable binding of spike protein to ACE2 is essential for virus entry, and the interactions between them should be understood well for the treatment modalities.

8.2. Introduction:

Coronavirus disease 2019 (COVID-19), a disease caused by the severe acute respiratory syndrome coronavirus 2 (SARS-CoV-2), has killed over 5.4 million people globally, making it the deadliest global health catastrophe since the 1918 influenza pandemic. The virus has continued to strike destruction since the World Health Organization (WHO) proclaimed it a global pandemic on March 11, 2020, with many countries seeing numerous waves of breakouts. The pathogenic capacity of a virus can be altered by adaptive mutations in its genome. Even a single amino acid substitution can have a significant impact on a virus's ability to elude the immune system, making vaccine development difficult. SARS-CoV-2, like other RNA viruses, is prone to genetic evolution as it adapts to new human hosts, resulting in the creation of various variants with distinct characteristics than the ancestral strains. Periodic genomic sequencing of viral samples aids in the detection of new SARS-CoV-2 genetic variations circulating in populations, particularly in the event of a worldwide pandemic. During the early stages of the pandemic, SARS-genetic CoV-2's evolution was limited, with the exception of the appearance of a worldwide

dominant variant known as D614G, which was linked to higher transmissibility but not increased disease severity compared to its ancestral strain. Another human variant, linked to infection of farmed mink in Denmark, was discovered, although it was not linked to greater transmissibility. Multiple SARS-CoV-2 variants have been identified since then, with a number of them being classified as variants of concern (VOCs) due to their public health implications. VOCs have been linked to increased transmissibility or virulence, decreased neutralization by antibodies obtained from natural infection or vaccination, the potential to elude detection, and a reduction in therapeutic or vaccine efficiency. Five SARS-CoV-2 VOCs (Alpha (B.1.1.7), Beta (B.1.351), Gamma (P.1), Delta (B.1.617.2) and Omicron (B.1.1.529)) have been detected since the start of the pandemic, according to a recent WHO epidemiological update, as of December 11, 2021. The fourth variant of concern, B.1.617.2 (also known as the Delta variant), was first discovered in India in December 2020 and was responsible for the deadly second wave of COVID-19 infections in India in April 2021. This variant was first found in the United States in March 2021, and it has turned into the most prevalent SARS-CoV-2 strain in the country. With cases reported in over 96 countries, the spread of the delta variant, which originated in India [1] has generated concern all over the world. Many countries, including the United States, Africa, Brazil, Australia and Europe, are threatened by these variants. India is still fighting a resurgence of the delta variant which appeared in the early part of 2021. The Delta variant has reported to evade neutralizing antibodies and is believed to be 60% more transmissible than the already highly infectious Alpha variant (B.1.1.7) [1,2], The recent studies on the variant have ignited fresh attention into how SARS-CoV-2 is able to adapt and mutate with the existing environment [3]. Another variant which is very similar to the Delta variant is the Delta Plus variant (AY.1) which was first detected in Europe and was declared as a “variant of concern” by the U.K. governmental agency Health England. The delta Plus variant is a sub lineage of the delta variant, with a notable difference of possessing K417N mutation in the spike protein. The majority of the changes in these variants have occurred in the RBD domain of the spike protein [4, 5], and these alterations correspond to improved virus transmissibility [6, 7], evasion [8,9] and flexibility in the spike protein’s interaction with the host receptors [10]. Due to decreased vaccination efficacy due to mutations and the lack of viable antiviral medication candidate against SARS-CoV-2, the globe is still fighting to defeat the pandemic. With decrease in vaccine efficacy due to mutations [11] and the absence of strong anti-viral drug candidate against SARS-CoV-2, the world is still battling to overcome the Pandemic. In this situation, one can look into nature for a cure and a solution [12-33]. The mutations present in the RBD region of the spike protein of Delta and Delta Plus variants may affect its binding affinity to human cell-surface protein angiotensin I-converting enzyme 2 (ACE2). Modifications in the spike protein’s

RBD region may lead to changes in the virus's ACE2 binding specificity and alter its antigenicity, that is, recognition by immune antibodies. Here, we seek to investigate the binding interactions between RBD region of spike protein of Delta and Delta Plus variants of SARS-CoV-2 with the ACE2 by employing MD simulation and other computational approaches.

8.3. Materials and Methods:

The initial 3-D structure of SARS-CoV-2 spike receptor-binding domain bound with ACE2 (S protein-ACE2) (PDB ID: 6lzg with a resolution of 2.50 Å) was retrieved from the Research Collaboratory for Structural Bioinformatics Protein Data bank (www.rcsb.org) [34]. The 3-D structure of the SARS-CoV-2 receptor-binding domain of Delta (L452R and T478K) (**Figure 8.1A)** and Delta-Plus (L452R, K417N and T478K) **(Figure 8.1B)** variants bound with ACE2 were obtained by inducing punctual mutation of PDB: 6lzg crystal structure using UCSF Chimera package alpha v.1.12 [35]. Both the complex structures were then energy minimized using steepest descents followed by conjugate gradient minimization.

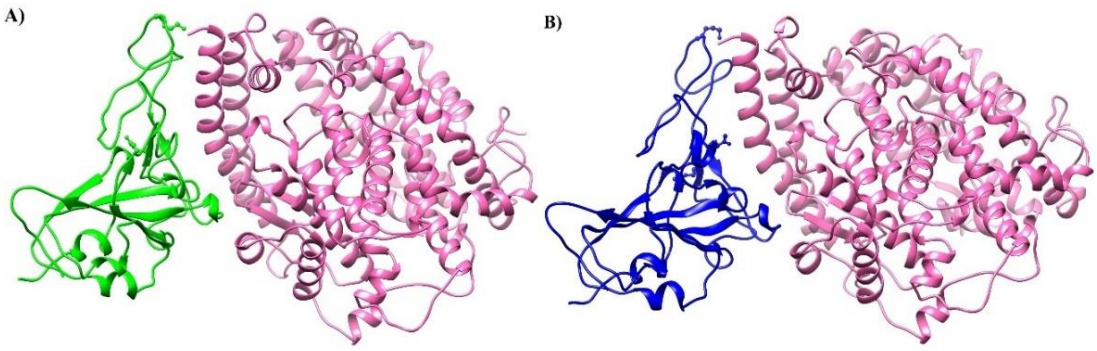

Figure 8.1. *Three dimensional structure of* ***(A)*** *SARS-CoV-2 spike receptor-binding domain Delta variant bound with ACE2 (S protein(Delta)-ACE2)* ***(B)*** *SARS-CoV-2 spike receptor-binding domain Delta Plus variant bound with ACE2 (S protein(Delta Plus)-ACE2)*

8.3.1. Molecular Dynamics Simulations.

The Delta as well as the Delta-Plus variants of the complex of SARS-CoV-2 spike receptor-binding domain bound with ACE2 were subjected to MD simulations. The MD simulation was performed using AMBER ff14SB force field [36] with AMBER software package [36]. To ensure the overall neutrality of the two complex systems, appropriate numbers of counter ions were added. The two complex systems were subjected to MD simulations in explicit solvent, and were solvated with TIP3P [37] water model

with a solvent buffer of 10 Å in all directions. In the first step of minimization, spike receptor-binding domain and ACE2 were fixed with a 500 kcal/mol/Å^2, and minimized the energy of all water molecules and counterions for 10000 steps of steepest descents (SD) followed by 10000 steps of the conjugate gradient (CG). Subsequently in the second step of minimization, to remove conflicting contacts the entire complex systems was repeated for 12000 steps of SD minimization and 8000 steps of CG minimization. Next, both the complex syste ms were gradually heated from 0-300 K in constant volume (NVT) conditions, thereby applying harmonic restraints with a force constant of 10 kcal/mol/Å^2 on the solute atoms, and equilibration was performed three times with 3000 ps using a force constant of 5.0 kcal/mol/Å. Finally, 100 ns MD simulations were performed using the NPT ensemble without restraints. We used the Particle mesh Ewald [38,39] technique with a non-bonded cutoff of 12.0 Å to limit the direct space sum to treat the long-range electrostatic interactions. All the bonds present in the system were constrained using the SHAKE algorithm [41]. The pressure and temperature (0.5 ps of heat bath and 0.2 ps of pressure relaxation) were kept constant by the Berendsen weak coupling algorithm [40] throughout the simulation process. The time step of MD simulation was set to 2 fs, and sampling was performed every 10 ps into the MD file.

After completion of the 100 ns of production dynamics of the complexes, the lowest energy conformer of the individual complex (S protein(Delta)-ACE2 and S protein(Delta-Plus)-ACE2) was extracted out using the RMSD clustering algorithm from the highly populated clusters and submitted to PDBsum server (http://www.ebi.ac.uk/thornton-srv/databases/pdbsum/Generate.html) to analyse for their residue-specific interactions which are considered to be important to know about the nature of interactions. PDBsum [42] is a database that, among other things, shows schematic diagrams of the non-bonded contacts between amino acid residues at the interface of molecules in a multimer complex.

8.3.2. Binding Free energy calculations.

The Molecular Mechanics Poisson−Boltzmann Surface Area (MM-PBSA) and Molecular Mechanics Generalized Born Surface Area (MM-GBSA) method [43,44] implemented in AMBER 16 package was performed to calculate the binding free energy as well as the free energy decomposition of the two complex systems (S protein(Delta)-ACE2 and S protein(Delta-Plus)-ACE2). For each complex system, 200 snapshots were selected from the last 10 ns of MD trajectories to calculate the relevant energies.

The formulas for calculating the BFE and their decomposed energetic components are same as described in the 7A.3.2 section of Chapter 7A [45,46]. The entropy was also estimated with normal mode (nmode) analysis [47]. The approaches and protocols that we have considered in this study to estimate the binding free energy have been used in many of the recent *in-silico* studies [48-55].

8.4. Results and Discussion:

During the month of May, 2021, India has faced the world's most devastating wave of coronavirus infections since the start of the COVID-19 pandemic. The situation remained grim as the country records a staggering number of daily new infections at around four lakhs. Despite the pain and suffering, scientists are working round the clock to identify the reason for such a 'tsunami' of the cases. And one of the main suspects remains the emergence of the more virulent mutant variants of the coronavirus. The new Delta-Plus variant from India carries the genetic code from two other mutations, T478K and L452R, which were already circulating globally. While both the mutations, traced across separate variants are characteristic for their high infectivity and transmission rates, this is the first time they have merged, making it many times more infectious and deadly. The mutations in this variant are expected therefore to develop resistant to antibodies that are generated by vaccination or by natural infection. However, the impact of this newly reported variant has not yet been investigated. Here, we performed a computational study to investigate the effect of these mutations on the binding affinity of spike protein for ACE2 and its impact on the transmission.

8.4.1. MD simulation.

The RBD domain of wild type strain of COVID-19 has been explored, and the structure of this SARS-CoV-2 spike receptor binding domain bound with ACE2 protein has been reported. From the wild type structure of SARS-CoV-2 spike receptor-binding domain bound with ACE2, the 3-D structure of the Delta (L452R and T478K) and Delta-Plus (L452R, K417N and T478K) of SARS-CoV-2 spike receptor-binding domain bound with ACE2 were obtained by punctual mutation. Then the energy minimization was carried out on both the complex structures using steepest descents followed by conjugate gradient minimization. Both the complexes were then submitted to MD simulations with AMBER program.

8.4.1.1. RMSD Analysis.

To test the stability of the (S protein (Delta)-ACE2) and (S protein (Delta-Plus)-ACE2) complexes, 100 ns of MD simulation studies were carried out. The conformational snapshots of the (S protein (Delta)-ACE2) and (S protein (Delta-Plus)-ACE2) complexes during the course of 100 ns MD simulation time

were depicted in **Figure 8.2** and **Figure 8.3**.

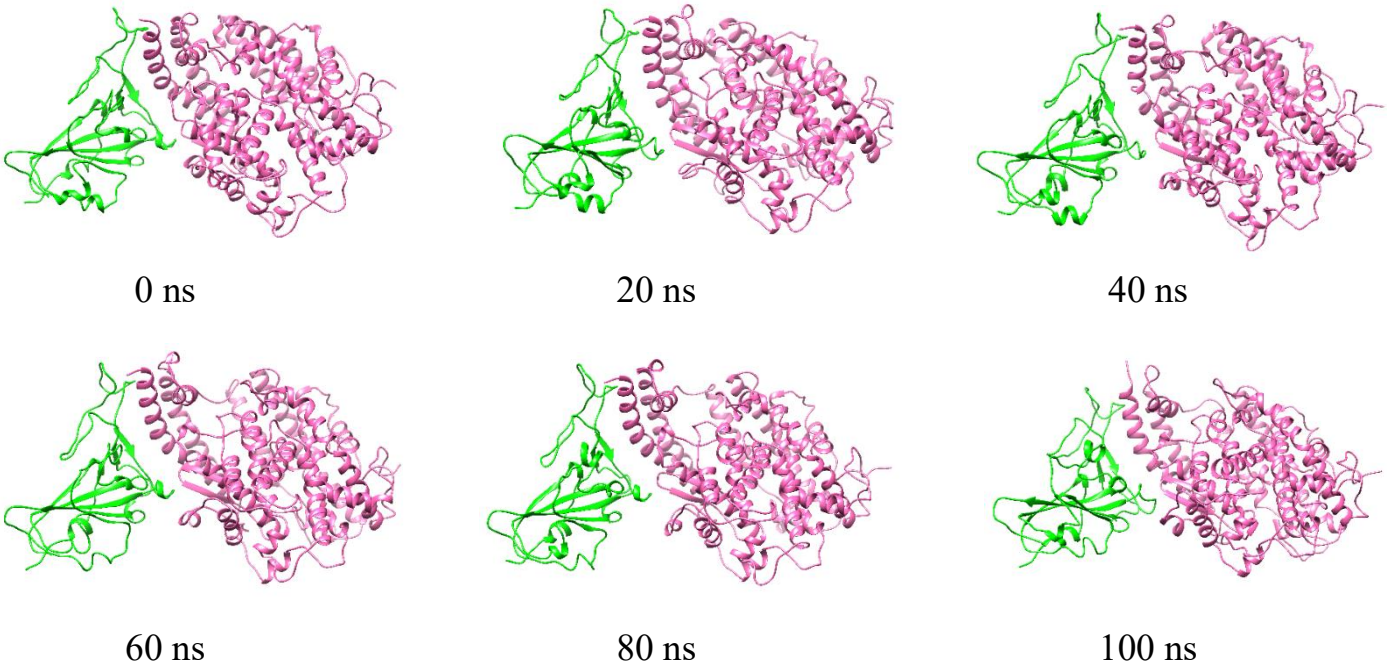

Figure 8.2. *Snapshots of SARS-CoV-2 ACE2-Spike Protein (Delta variant) structures at discrete distance of separation (in Å) between their centre of mass.*

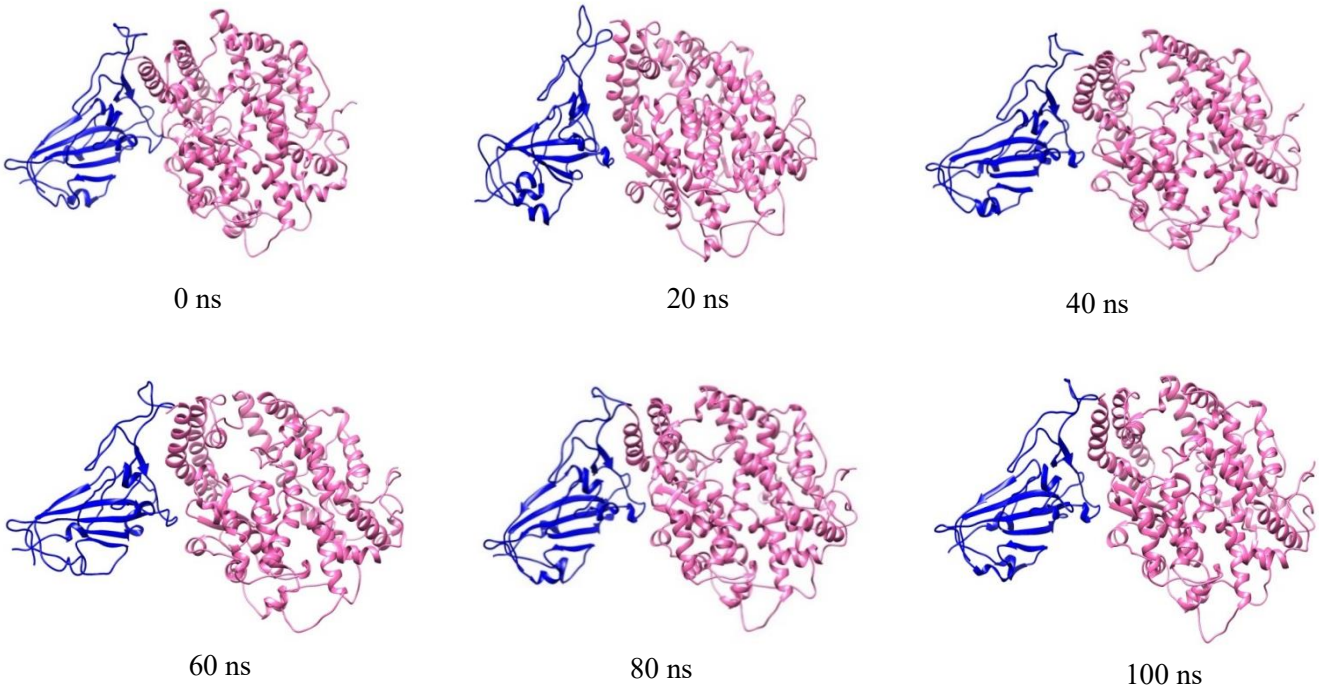

Figure 8.3. *Snapshots of SARS-CoV-2 ACE2-Spike Protein (Delta-plus variant) structures at discrete distance of separation (in Å) between their centre of mass.*

The average deviations in the atomic positions and the stability through the trajectory of 100 ns of the MD simulations, the RMSD (root mean square deviation) values of the backbone atoms of the complexes along with the S protein (Apo form) were calculated (**Figure 8.4**).

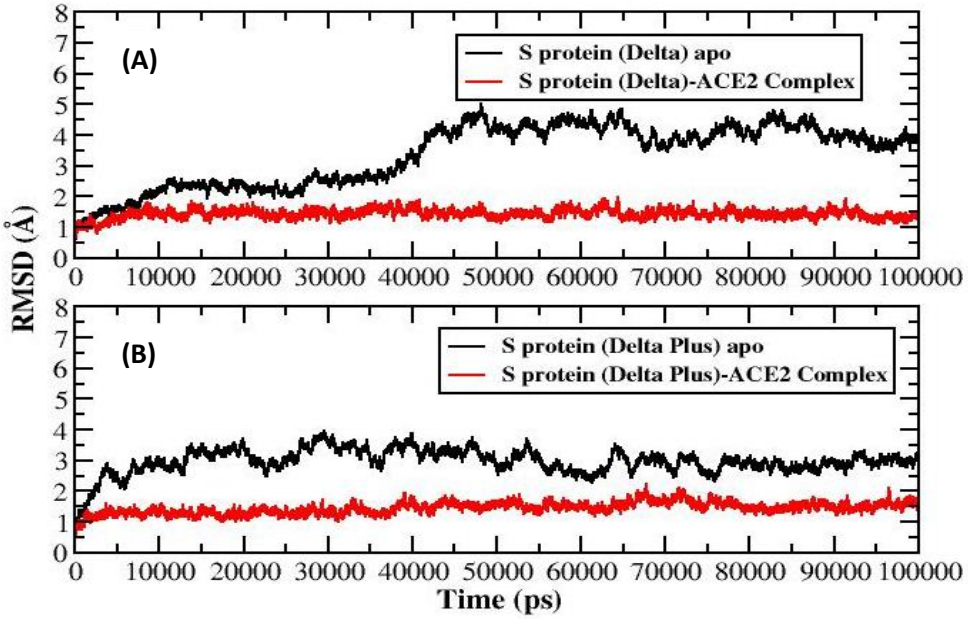

Figure 8.4. *Backbone RMSD's for* ***(A)*** *S protein (Delta) Apo (black), S protein (Delta)-ACE2 complex (red)* ***(B)*** *S protein (Delta-Plus) Apo (black), S protein (Delta-Plus)-ACE2 complex (red).*

The RMSD of Delta type as well as the Delta-Plus complex appeared to be stable after 10 ns, revealing that good convergence was achieved for each system. Interestingly, we noticed the RMSD values of the Delta and Delta-Plus complexes to depict lower values and observed to be stable. The average of RMSD is 1.84 Å (± 0.12) for the Delta type complex structure and 1.42 Å (± 0.14) for the Delta-Plus complex structure, which could indicate greater stability of the mutated complex structure. We have also compared the average deviations in the atomic positions of the residues exclusively at the mutation sites 452 and 478 (**Figure 8.5**). At residue index 452 and 478, we observed RMSD fluctuations to be relatively lower in the case of Delta and Delta-Plus complexes than in the Wild type complex. RMSD plot of the residue at position 417 in S protein (WILD)-ACE2 complex (black) and S protein (Delta-Plus)-ACE2 complex (green) was also analyzed **(Figure 8.6)** and found the RMSD fluctuations to be lower in Delta-Plus complex. We also noticed that the binding of ACE2 reduced the perturbation of S protein to a significant extent in both Delta and Delta-Plus complex systems.

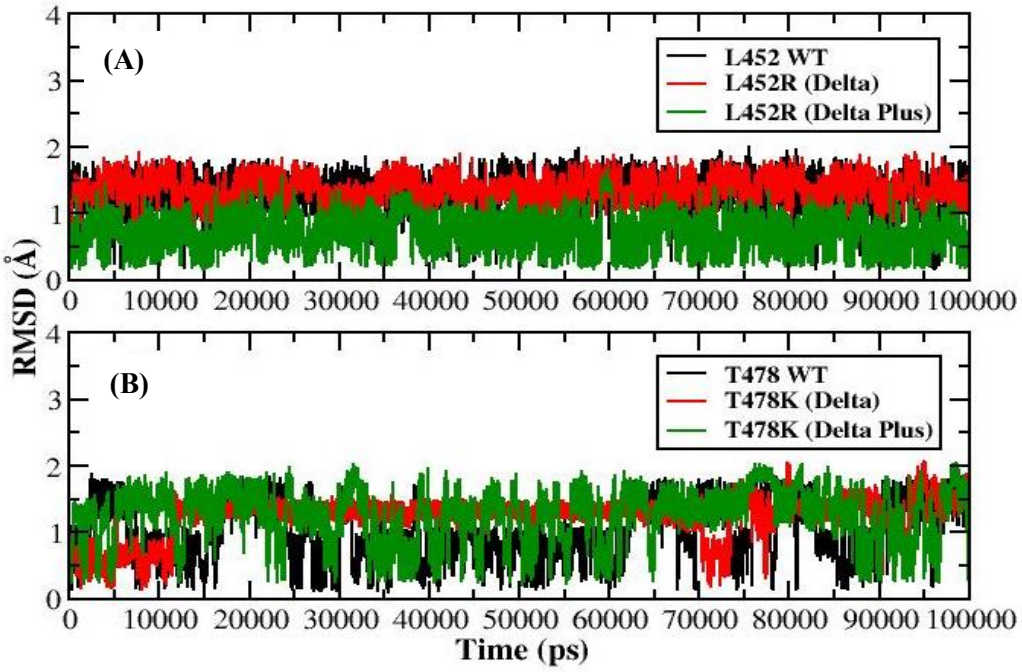

Figure 8.5. *RMSD plot of the residue at position* ***(A)*** *452* ***(B)*** *478 in S protein (WILD)-ACE2 complex (black), S protein (Delta)-ACE2 complex (red) and S protein (Delta-Plus)-ACE2 complex (green)*

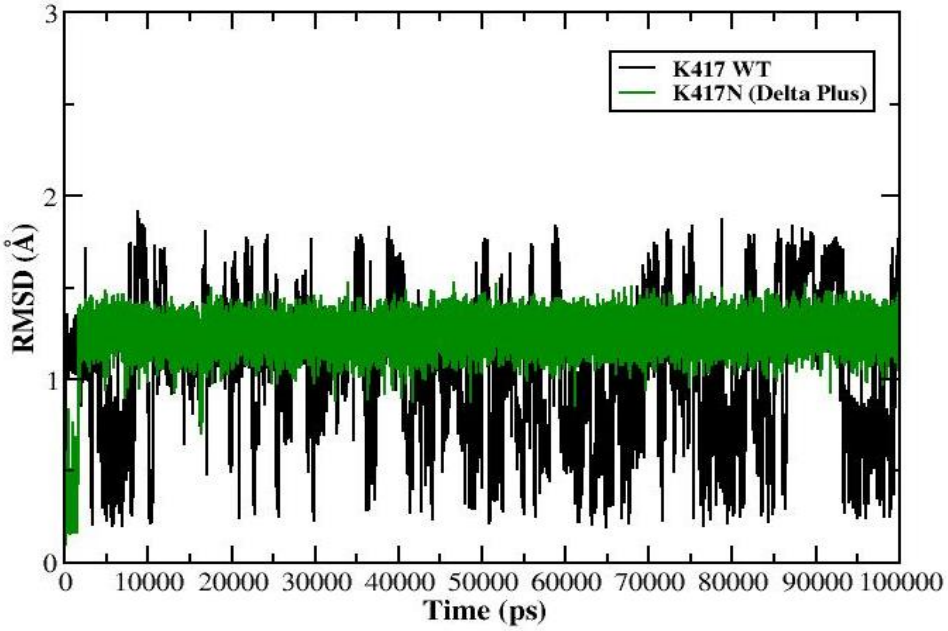

Figure 8.6. *RMSD plot of the residue at position 417 in S protein (WILD)-ACE2 complex (black) and S protein (Delta-Plus)-ACE2 complex (green)*

8.4.1.2. RMSF Analysis

We further explored the S protein flexibility by RMSF values of the Cα from the MD simulations of the (S protein (Delta)-ACE2) and (S protein (Delta-Plus)-ACE2) complexes (**Figure 8.7**). We observed significant differences in the flexibility of S protein in Delta and Delta-Plus complexes in particular at the region in and around the mutation position (452, 478 and 417). The RMSF values of the Cα atoms of S protein in Delta and Delta-Plus complexes shows relatively lower values than in Wild-type complex (Chapter 7A). From **Figure 8.7**, it is more apparent that there is significant reduction in structural fluctuations and increased stability in the case of Delta and Delta-Plus complexes.

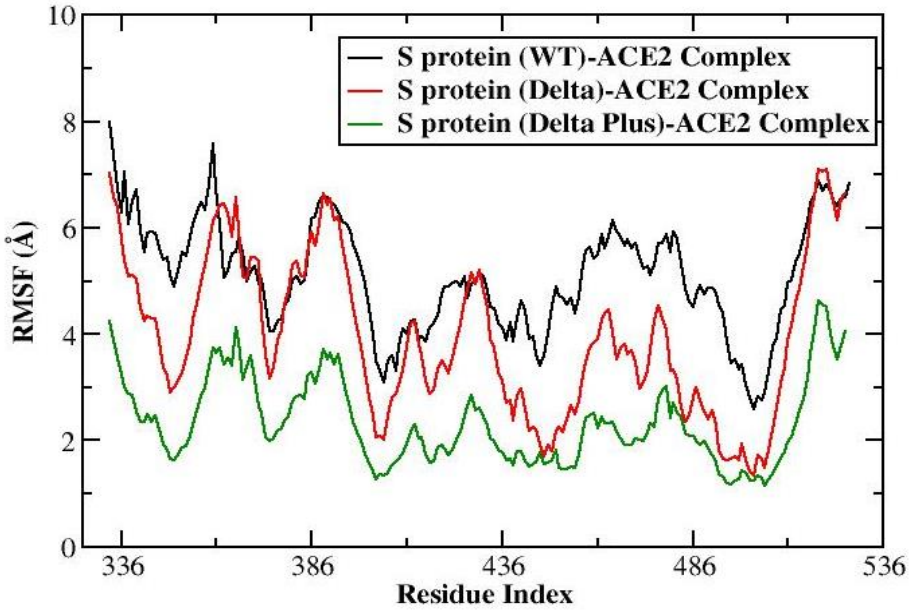

Figure 8.7. *Backbone RMSF's for S protein in S protein (WILD)-ACE2 complex (black), S protein (Delta)-ACE2 complex (red) and S protein (Delta-Plus)-ACE2 complex (green)*

8.4.1.3. Hydrogen bond Analysis

Additionally, we also calculated and plotted the number of intermolecular hydrogen bonds present in the (S protein (Delta)-ACE2) and (S protein (Delta-Plus)-ACE2) complexes (**Figure 8.8**), as these hydrogen bonds play a crucial role in conferring the stability to the protein complexes. The number of inter-molecular hydrogen bonds were found to be higher in S protein (Delta-Plus)-ACE2 and S protein (Delta)-ACE2 complex.

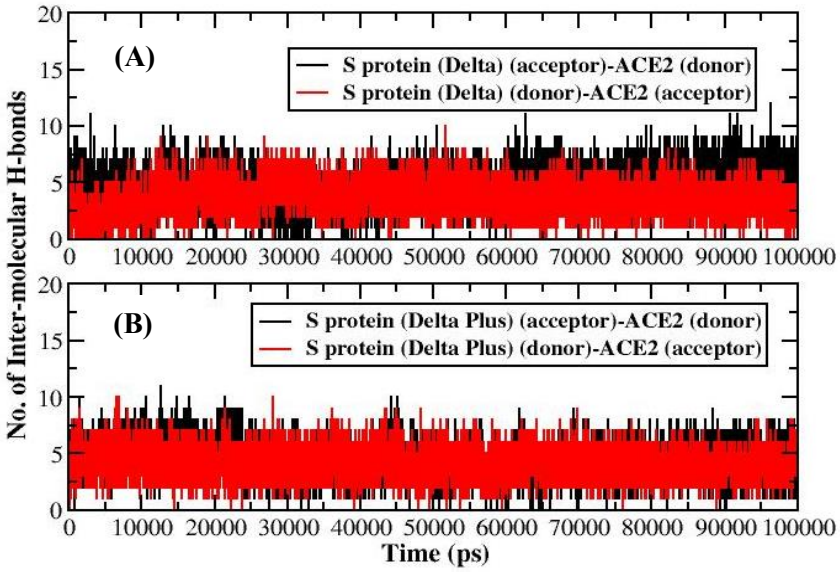

Figure 8.8. *Number of intermolecular hydrogen bonds between S protein and ACE2 in* ***A)*** *S protein (Delta)-ACE2 complex* ***B)*** *S protein (Delta-Plus)-ACE2 complex*

The list of intermolecular hydrogen bonds noticed between the S protein (acceptor/donor) and ACE2 (donor/acceptor) during the last 20 ns of MD simulation of the Delta and Delta-Plus complexes were summarized in **Table 8.1-8.4**.

Table 8.1. *Hydrogen bond analysis of S protein (DELTA)-ACE2 complex during the last 20 ns of MD simulation with S protein as acceptor and ACE2 as donor*

#Acceptor	DonorH	Donor	Frac	Average Distance (Å)	Average Angles (°)
GLN_498@OE1	GLN_42@HE21	GLN_42@NE2	0.5507	2.8653	162.2189
GLN_498@OE1	LYS_353@HZ2	LYS_353@NZ	0.3066	2.8136	159.1395
GLN_498@OE1	LYS_353@HZ1	LYS_353@NZ	0.2856	2.8066	156.3792
GLN_493@OE1	LYS_31@HZ1	LYS_31@NZ	0.1892	2.7974	158.1674
GLN_493@OE1	LYS_31@HZ2	LYS_31@NZ	0.1814	2.8015	158.5917
GLN_498@OE1	LYS_353@HZ3	LYS_353@NZ	0.1814	2.8075	156.0259
ALA_475@O	GLN_24@HE22	GLN_24@NE2	0.1598	2.8663	156.5649
GLN_493@OE1	LYS_31@HZ3	LYS_31@NZ	0.1472	2.8018	158.6927
ASN_501@OD1	LYS_353@HZ3	LYS_353@NZ	0.1373	2.8063	149.3355
ALA_475@O	SER_19@H2	SER_19@N	0.0741	2.8471	153.6287
TYR_489@OH	TYR_83@HH	TYR_83@OH	0.0725	2.8337	155.5629
ALA_475@O	SER_19@H3	SER_19@N	0.0704	2.8454	153.7257
ASN_501@OD1	LYS_353@HZ2	LYS_353@NZ	0.0684	2.8117	150.3018
LEU_492@O	LYS_31@HZ3	LYS_31@NZ	0.0641	2.8284	151.3374
GLY_502@HA3	GLY_354@HA3	GLY_354@CA	0.0593	2.9211	141.7867
GLU_484@OE1	LYS_31@HZ1	LYS_31@NZ	0.0575	2.7989	153.0558
LEU_492@O	LYS_31@HZ2	LYS_31@NZ	0.0559	2.8233	150.5004
LEU_492@O	LYS_31@HZ1	LYS_31@NZ	0.0556	2.8285	151.0206
ALA_475@O	SER_19@H1	SER_19@N	0.0553	2.8421	153.8468

ALA_475@O	SER_19@HG	SER_19@OG	0.0476	2.713	161.3645
GLY_496@O	LYS_353@HZ3	LYS_353@NZ	0.0454	2.8587	153.6011
PHE_490@O	LYS_31@HZ2	LYS_31@NZ	0.0439	2.855	152.2969
GLU_484@OE1	LYS_31@HZ2	LYS_31@NZ	0.0407	2.7942	151.9281
GLU_484@OE1	LYS_31@HZ3	LYS_31@NZ	0.0394	2.8022	152.7312
PHE_490@O	LYS_31@HZ3	LYS_31@NZ	0.0333	2.8631	153.6305
TYR_489@HE1	PHE_28@HB2	PHE_28@CB	0.0276	2.9389	139.9999
GLU_484@OE2	LYS_31@HZ1	LYS_31@NZ	0.0271	2.8381	151.5963
GLY_496@O	LYS_353@HZ2	LYS_353@NZ	0.0248	2.8564	154.3297
GLU_484@OE2	LYS_31@HZ2	LYS_31@NZ	0.0241	2.8329	152.6549
GLN_493@HE21	GLU_35@HB2	GLU_35@CB	0.023	2.871	146.8194
GLU_484@OE2	LYS_31@HZ3	LYS_31@NZ	0.0182	2.8353	152.8463
TYR_489@HH	PHE_28@HB2	PHE_28@CB	0.0182	2.8842	151.9685
THR_500@O	ASN_330@HD21	ASN_330@ND2	0.0153	2.8748	146.8897
PHE_490@O	LYS_31@HZ1	LYS_31@NZ	0.0152	2.8769	151.5013
THR_500@HG1	ARG_357@HH21	ARG_357@NH2	0.0132	2.8624	139.8828
PHE_490@HB3	LYS_31@HE3	LYS_31@CE	0.0132	2.8944	144.6722
GLY_496@O	LYS_353@HZ1	LYS_353@NZ	0.0126	2.873	154.5785
PHE_490@H	LYS_31@HE3	LYS_31@CE	0.0112	2.902	152.8467
ASN_501@OD1	LYS_353@HZ1	LYS_353@NZ	0.0088	2.8302	150.9196
PHE_490@HB3	LYS_31@HE2	LYS_31@CE	0.0082	2.9014	145.6414
TYR_489@HH	LEU_79@HD21	LEU_79@CD2	0.0078	2.8133	148.1638
TYR_449@HH	GLN_42@HE22	GLN_42@NE2	0.007	2.8976	142.1551
TYR_489@HH	LEU_79@HD22	LEU_79@CD2	0.007	2.8214	148.9876
TYR_449@OH	GLN_42@HE22	GLN_42@NE2	0.0069	2.9052	150.3965
THR_500@HG1	TYR_41@HH	TYR_41@OH	0.0064	2.8204	141.0035

Table 8.2. *Hydrogen bond analysis of S protein (DELTA)-ACE2 complex during the last 20 ns of MD simulation with S protein as donor and ACE2 as acceptor*

#Acceptor	DonorH	Donor	Frac	Average Distance (Å)	Average Angles (°)
ASP_38@OD1	TYR_449@HH	TYR_449@OH	0.6236	2.693	161.9246
LYS_353@O	GLY_502@H	GLY_502@N	0.5714	2.8778	159.9073
TYR_41@OH	THR_500@HG1	THR_500@OG1	0.4712	2.8014	158.9853
GLN_42@OE1	GLN_498@HE21	GLN_498@NE2	0.4653	2.8757	162.1953
GLU_35@OE1	GLN_493@HE21	GLN_493@NE2	0.3831	2.8265	159.8379
GLU_35@OE2	GLN_493@HE21	GLN_493@NE2	0.2372	2.829	159.9659
ASP_355@OD2	THR_500@HG1	THR_500@OG1	0.224	2.7243	162.1695
ASP_38@OD2	TYR_449@HH	TYR_449@OH	0.21	2.7279	160.7297
GLN_24@O	TYR_489@HH	TYR_489@OH	0.1513	2.812	145.4541
TYR_83@OH	ASN_487@H	ASN_487@N	0.1092	2.9232	161.806
TYR_83@OH	TYR_489@HH	TYR_489@OH	0.1014	2.8629	150.6138
ASP_30@OD1	LYS_417@HZ3	LYS_417@NZ	0.0943	2.7749	157.7357
TYR_41@HH	THR_500@HG1	THR_500@OG1	0.0693	2.871	146.7438
ASP_30@OD1	LYS_417@HZ2	LYS_417@NZ	0.0643	2.787	157.1344
GLY_354@HA3	GLY_502@HA3	GLY_502@CA	0.0557	2.9291	145.3736
HIE_34@O	GLN_493@HE22	GLN_493@NE2	0.0471	2.8642	154.2906
ASP_30@OD2	LYS_417@HZ2	LYS_417@NZ	0.0469	2.7815	156.2563

ASP_30@OD2	LYS_417@HZ3	LYS_417@NZ	0.0469	2.7831	157.8188
ASP_30@OD2	LYS_417@HZ1	LYS_417@NZ	0.0462	2.7878	157.5149
ASP_30@OD1	LYS_417@HZ1	LYS_417@NZ	0.0374	2.7788	156.1463
PHE_28@HB2	TYR_489@HH	TYR_489@OH	0.0348	2.8493	147.7873
TYR_83@HH	ASN_487@H	ASN_487@N	0.0259	2.9216	157.6922
PHE_28@HB2	TYR_489@HE1	TYR_489@CE1	0.0248	2.9497	145.6507
GLU_35@HB2	GLN_493@HE21	GLN_493@NE2	0.0205	2.8175	146.1815
LYS_31@HE3	PHE_490@HB3	PHE_490@CB	0.0174	2.9047	145.5947
LEU_79@HD21	TYR_489@HH	TYR_489@OH	0.0143	2.7658	153.9927
LEU_79@HD22	TYR_489@HH	TYR_489@OH	0.0127	2.7855	155.1003
GLU_35@HG2	GLN_493@HE21	GLN_493@NE2	0.0107	2.8125	147.6822
ALA_386@O	TYR_505@HH	TYR_505@OH	0.0107	2.7603	159.2593
TYR_41@HE2	THR_500@HG1	THR_500@OG1	0.0097	2.8635	144.891
LYS_31@HE2	PHE_490@HB3	PHE_490@CB	0.0097	2.9153	148.846
TYR_41@HE2	GLN_498@HE21	GLN_498@NE2	0.0083	2.8734	149.6651
LEU_79@HD23	TYR_489@HH	TYR_489@OH	0.0073	2.7824	152.5098
GLU_35@OE1	SER_494@HG	SER_494@OG	0.0066	2.7107	164.1631
LYS_31@HE3	PHE_490@H	PHE_490@N	0.0066	2.8645	141.7725
ASN_330@HD21	THR_500@HB	THR_500@CB	0.0057	2.8388	145.4362
ARG_357@HH21	THR_500@HG1	THR_500@OG1	0.0056	2.8404	140.5976
GLN_24@HG2	ALA_475@HB3	ALA_475@CB	0.0053	2.95	141.54
HIE_34@HE2	LEU_455@HD13	LEU_455@CD1	0.0053	2.8941	144.1877

Table 8.3. *Hydrogen bond analysis of S protein (DELTA PLUS)-ACE2 complex during the last 20 ns of MD simulation with S protein as acceptor and ACE2 as donor*

#Acceptor	DonorH	Donor	Frac	Average Distance (Å)	Average Angles (°)
GLN_498@OE1	GLN_42@HE21	GLN_42@NE2	0.7617	2.85	162.6269
PHE_486@O	TYR_83@HH	TYR_83@OH	0.7469	2.7524	155.9339
GLN_498@OE1	LYS_353@HZ2	LYS_353@NZ	0.5296	2.796	154.6215
GLY_496@O	LYS_353@HZ3	LYS_353@NZ	0.4418	2.8306	155.7951
GLN_498@OE1	LYS_353@HZ3	LYS_353@NZ	0.2943	2.7992	155.7832
GLY_496@O	LYS_353@HZ1	LYS_353@NZ	0.266	2.8247	156.8619
ALA_475@O	SER_19@HG	SER_19@OG	0.0892	2.7309	159.9891
GLN_493@OE1	LYS_31@HZ3	LYS_31@NZ	0.0727	2.7803	156.3293
ALA_475@O	GLN_24@HE22	GLN_24@NE2	0.0712	2.8541	158.5407
GLY_502@HA3	GLY_354@HA3	GLY_354@CA	0.0509	2.9316	142.7164
GLN_498@OE1	LYS_353@HZ1	LYS_353@NZ	0.0393	2.7963	153.3046
GLN_493@OE1	LYS_31@HZ1	LYS_31@NZ	0.0389	2.7776	155.531
ALA_475@O	SER_19@H3	SER_19@N	0.0362	2.8325	152.5473
GLY_496@O	LYS_353@HZ2	LYS_353@NZ	0.0337	2.8355	155.6598
TYR_489@HB3	LYS_31@HE3	LYS_31@CE	0.0311	2.9013	147.7997
TYR_505@HH	ARG_393@HH22	ARG_393@NH2	0.0292	2.9091	144.1933
ALA_475@O	SER_19@H1	SER_19@N	0.0285	2.8338	152.6704
ALA_475@O	SER_19@H2	SER_19@N	0.0279	2.8292	152.2275
TYR_489@HH	PHE_28@HB2	PHE_28@CB	0.0276	2.8704	148.7951
GLN_493@OE1	LYS_31@HZ2	LYS_31@NZ	0.0276	2.7634	156.2306
TYR_489@HB2	LYS_31@HE3	LYS_31@CE	0.0267	2.9055	148.0868
THR_500@HG1	ARG_357@HH21	ARG_357@NH2	0.0225	2.8592	139.5305

ASN_501@OD1	LYS_353@HZ3	LYS_353@NZ	0.0225	2.8465	146.2969
PHE_490@O	LYS_31@HZ1	LYS_31@NZ	0.0221	2.8647	155.6311
TYR_490@OH	HIE_34@HE2	HIE_34@NE2	0.0192	2.8435	152.6456
GLN_493@HE21	GLU_34@HB2	GLU_34@CB	0.0186	2.8777	145.2207
GLU_484@OE2	LYS_31@HZ1	LYS_31@NZ	0.0162	2.7928	156.5559
SER_477@OG	GLN_24@HE21	GLN_24@NE2	0.0146	2.8861	157.1783
PHE_490@O	LYS_31@HZ3	LYS_31@NZ	0.013	2.8611	157.4532
ASN_501@HD21	LYS_353@HD2	LYS_353@CD	0.0118	2.9233	146.88
THR_500@HG1	TYR_41@HH	TYR_41@OH	0.0103	2.8102	140.0509
GLU_484@OE2	LYS_31@HZ2	LYS_31@NZ	0.01	2.8132	154.5051
PHE_490@HB3	LYS_31@HE3	LYS_31@CE	0.01	2.9018	144.1297
GLN_493@HE22	LYS_31@HE2	LYS_31@CE	0.0095	2.9085	154.2185
TYR_489@HH	PHE_28@HD1	PHE_28@CD1	0.0083	2.874	148.4554
PHE_490@O	LYS_31@HZ2	LYS_31@NZ	0.008	2.8577	157.392
TYR_505@OH	ARG_393@HH22	ARG_393@NH2	0.0077	2.9061	151.2319
THR_500@O	ASN_330@HD21	ASN_330@ND2	0.0076	2.889	148.8327
TYR_489@HE1	PHE_28@HB2	PHE_28@CB	0.007	2.9387	140.7699
ASN_487@HD21	GLN_24@HG2	GLN_24@CG	0.007	2.8726	146.6654
ASN_501@OD1	LYS_353@HE3	LYS_353@CE	0.0069	2.9642	141.6958
TYR_489@HH	TYR_83@HH	TYR_83@OH	0.0056	2.9113	143.0294
SER_477@OG	SER_19@HG	SER_19@OG	0.0053	2.7736	159.3709
GLU_484@OE2	LYS_31@HZ3	LYS_31@NZ	0.0052	2.7987	153.1001

Table 8.4. *Hydrogen bond analysis of S protein (DELTA PLUS)-ACE2 complex during the last 20 ns of MD simulation with S protein as donor and ACE2 as acceptor.*

#Acceptor	DonorH	Donor	Frac	Average Distance (Å)	Average Angles (°)
LYS_353@O	GLY_502@H	GLY_502@N	0.7457	2.8646	161.8695
GLN_42@OE1	GLN_498@HE21	GLN_498@NE2	0.5394	2.8778	162.0907
ASP_355@OD1	THR_500@HG1	THR_500@OG1	0.5362	2.7176	161.986
GLU_37@OE1	TYR_505@HH	TYR_505@OH	0.3708	2.7545	158.3531
GLU_35@OE1	GLN_493@HE21	GLN_493@NE2	0.324	2.8351	161.1112
GLU_35@OE2	GLN_493@HE21	GLN_493@NE2	0.3167	2.8327	160.5401
TYR_41@OH	THR_500@HG1	THR_500@OG1	0.3115	2.7967	159.4389
ASP_38@OD2	TYR_449@HH	TYR_449@OH	0.2225	2.6572	165.2554
GLN_24@OE1	ASN_487@HD21	ASN_487@ND2	0.2041	2.8419	154.2866
GLN_24@OE1	ASN_487@HD22	ASN_487@ND2	0.1991	2.8281	159.9813
TYR_41@HH	THR_500@HG1	THR_500@OG1	0.0753	2.8559	145.6898
GLY_354@HA3	GLY_502@HA3	GLY_502@CA	0.0466	2.929	142.0585
GLU_37@OE2	TYR_505@HH	TYR_505@OH	0.0416	2.7415	158.9966
TYR_83@OH	ASN_487@HD22	ASN_487@ND2	0.0343	2.9069	158.8668
GLN_24@O	TYR_489@HH	TYR_489@OH	0.0285	2.8375	146.1125
PHE_28@HB2	TYR_489@HH	TYR_489@OH	0.0236	2.7997	146.9589
ARG_357@HH21	THR_500@HG1	THR_500@OG1	0.019	2.8474	140.4169
LYS_31@HE3	TYR_489@HB3	TYR_489@CB	0.0172	2.8971	146.0249
ASN_330@HD21	THR_500@HB	THR_500@CB	0.0154	2.8729	148.8812
TYR_83@OH	TYR_489@HH	TYR_489@OH	0.0138	2.8786	145.4164
GLU_35@HB2	GLN_493@HE21	GLN_493@NE2	0.0129	2.8044	144.4727

LYS_31@HE3	PHE_490@HB3	PHE_490@CB	0.012	2.9147	147.2295
GLN_24@HG2	ASN_487@HD21	ASN_487@ND2	0.0115	2.8459	147.0977
ASP_38@OD1	TYR_449@HH	TYR_449@OH	0.0111	2.7789	159.8995
TYR_83@HH	TYR_489@HH	TYR_489@OH	0.0106	2.8668	143.9956
HIE_34@O	GLN_493@HE21	GLN_493@NE2	0.0096	2.8603	158.2311
HIE_34@HB2	GLN_493@HE21	GLN_493@NE2	0.0083	2.8558	153.1276
GLU_35@OE1	GLN_493@HE22	GLN_493@NE2	0.008	2.8266	158.906
LYS_31@HE3	TYR_489@HB2	TYR_489@CB	0.0075	2.8893	144.6467
LYS_353@HD2	ASN_501@HD21	ASN_501@ND2	0.0072	2.8639	140.2198
HIE_34@HB3	GLN_493@HE21	GLN_493@NE2	0.0071	2.8389	147.1803
PHE_28@HD1	TYR_489@HH	TYR_489@OH	0.0067	2.8022	144.713
PHE_28@HB2	TYR_489@HE1	TYR_489@CE1	0.0059	2.9491	143.6993
LYS_31@HD2	PHE_456@HE2	PHE_456@CE2	0.0056	2.9468	142.6428
GLN_24@HE21	SER_477@H	SER_477@N	0.0053	2.853	148.8498
GLU_35@HG2	GLN_493@HE21	GLN_493@NE2	0.005	2.8284	144.9133

8.4.1.4. Determination of the interface interactions of the S protein (Delta)-ACE2) and (S protein (Delta-Plus)-ACE2 complexes.

An interface area is usually defined as a region where two sets of proteins come in contact with each other. Surface residues with large surface regions accessible to the solvent available usually characterize them. The interface statistics for the S protein (Delta)-ACE2 and S protein (Delta-Plus)-ACE2 complexes were obtained upon the submission of the corresponding lowest energy complex structure extracted from the 100 ns MD simulation trajectory using RMSD clustering algorithm to the PDBsum server. The interface statistics for both the complexes have been shown in **Table 8.5**.

Table 8.5. *Interface statistics for the S protein (Delta)-ACE2 and S protein (Delta-Plus)-ACE2 complexes*

Complex system	**Chain**	**No. of interface residues**	**Interface area (Å^2)**	**No. of salt bridges**	**No. of disulphide bonds**	**No. of hydrogen bonds**	**No. of non-bonded contacts**
S protein (Delta)-ACE2	ACE2	19	916	2	-	15	149
	S protein (Delta)	20	921				
S protein (Delta Plus)-ACE2	ACE2	20	956	1	-	13	179
	S protein (Delta Plus)	20	969				

The detailed contributions of each interface residue stabilizing the Delta type and Delta-Plus complexes were summarized in **Table 8.6-8.11**. The total number of interface residues in the S protein (Delta)-ACE2 and S protein (Delta-Plus)-ACE2 complexes were found to be thirty-nine and forty respectively. In the S protein (Delta)-ACE2 complex, the interface area for the S protein chain and the ACE2 chain involved in the interaction was observed to be 916 $Å^2$ and 921 $Å^2$ respectively, while in the S protein (Delta-Plus)-ACE2 complex, the S protein chain and the ACE2 chain involved in the interaction was observed to be 956 $Å^2$ and 969 $Å^2$ respectively. Both the Delta and Delta-Plus complexes were stabilized by molecular interactions like salt bridges, hydrogen bonding, and non-bonded contacts. From **Table 8.6 - 8.11**, we can see the presence of one hundred and forty nine non-bonded contacts, two salt bridge and fifteen hydrogen bonds at the interface of S protein and ACE2 in the S protein (Delta)-ACE2 complex. However, at the interface of S protein and ACE2 in the S protein (Delta-Plus)-ACE2 complex, we observed one hundred and seventy-nine non-bonded contacts, one salt bridge and thirteen hydrogen bonds. Overall, we see the number of intermolecular interactions and the interface area shared by S protein and ACE2 in forming complex is larger in Delta-Plus complex than in the Delta type complex. Therefore, the stability of Delta-Plus complex was found to be higher than the Delta type complex.

***Table 8.6**. List of atom-atom interactions (Hydrogen bonds) across protein-ligand interface in ACE2 (Chain A)-Spike Protein (Chain B) (Delta variant) complex from PDBsum server*

ACE2						SARS-CoV-2 S protein (Delta)				
Sl. No	Atom no.	Atom name	Res name	Res no.	Hydrogen bonds	Atom no.	Atom name	Res name	Res no.	Distance
1	1	N	SER	19	<-->	6025	O	ALA	475	3.04
2	45	OE1	GLN	24	<-->	6106	ND2	ASN	487	2.79
3	94	OD2	ASP	30	<-->	5538	NZ	LYS	417	2.68
4	103	NZ	LYS	31	<-->	6083	OE2	GLU	484	2.8
5	103	NZ	LYS	31	<-->	6158	OE1	GLN	493	2.85
6	141	OE2	GLU	35	<-->	6159	NE2	GLN	493	2.74
7	163	OD2	ASP	38	<-->	5787	OH	TYR	449	2.53
8	192	OH	TYR	41	<-->	6215	OG1	THR	500	2.74
9	192	OH	TYR	41	<-->	6215	OG1	THR	500	2.74
10	203	NE2	GLN	42	<-->	5767	O	GLY	446	2.83
11	203	NE2	GLN	42	<-->	5787	OH	TYR	449	2.85
12	530	OH	TYR	83	<-->	6105	OD1	ASN	487	3.3
13	2725	O	LYS	353	<-->	6226	N	GLY	502	2.82
14	2723	NZ	LYS	353	<-->	6183	O	GLY	496	2.84
15	2723	NZ	LYS	353	<-->	6200	OE1	GLN	498	2.78

Table 8.7*. List of atom-atom interactions (Non-bonded contacts) across protein-ligand interface in ACE2 (Chain A)-Spike Protein (Chain B) (Delta variant) complex from PDBsum server*

ACE2					Non-bonded contacts	SARS-CoV-2 S protein (Delta)				
Sl.no.	Atom no.	Atom name	Res name	Res no.		Atom no.	Atom name	Res name	Res no.	Distance
1	1	N	SER	19	<-->	6025	O	ALA	475	3.04
2	43	CG	GLN	24	<-->	6025	O	ALA	475	3.44
3	43	CG	GLN	24	<-->	6106	ND2	ASN	487	3.89
4	44	CD	GLN	24	<-->	6104	CG	ASN	487	3.86
5	44	CD	GLN	24	<-->	6106	ND2	ASN	487	3.09
6	45	OE1	GLN	24	<-->	6027	CA	GLY	476	3.34
7	45	OE1	GLN	24	<-->	6104	CG	ASN	487	3.77
8	45	OE1	GLN	24	<-->	6106	ND2	ASN	487	2.79
9	46	NE2	GLN	24	<-->	6106	ND2	ASN	487	3.38
10	68	C	THR	27	<-->	6123	CE2	TYR	489	3.74
11	69	O	THR	27	<-->	5860	CZ	PHE	456	3.55
12	69	O	THR	27	<-->	6123	CE2	TYR	489	3.6
13	67	OG1	THR	27	<-->	5858	CD1	PHE	456	3.6
14	67	OG1	THR	27	<-->	5859	CE1	PHE	456	3.07
15	67	OG1	THR	27	<-->	5860	CZ	PHE	456	3.38
16	67	OG1	THR	27	<-->	6008	CE2	TYR	473	3.85
17	67	OG1	THR	27	<-->	6124	CD2	TYR	489	3.79
18	67	OG1	THR	27	<-->	6123	CE2	TYR	489	3.49
19	66	CG2	THR	27	<-->	6023	CB	ALA	475	3.31
20	70	N	PHE	28	<-->	6122	OH	TYR	489	3.69
21	71	CA	PHE	28	<-->	6122	OH	TYR	489	3.46
22	72	CB	PHE	28	<-->	6122	OH	TYR	489	3.43
23	95	C	ASP	30	<-->	5851	CD2	LEU	455	3.85
24	96	O	ASP	30	<-->	5851	CD2	LEU	455	3.74
25	92	CG	ASP	30	<-->	5538	NZ	LYS	417	3.8
26	93	OD1	ASP	30	<-->	5850	CD1	LEU	455	3.79
27	94	OD2	ASP	30	<-->	5537	CE	LYS	417	3.19
28	94	OD2	ASP	30	<-->	5538	NZ	LYS	417	2.68
29	94	OD2	ASP	30	<-->	5849	CG	LEU	455	3.86
30	94	OD2	ASP	30	<-->	5850	CD1	LEU	455	3.89
31	94	OD2	ASP	30	<-->	5859	CE1	PHE	456	3.44
32	101	CD	LYS	31	<-->	6158	OE1	GLN	493	3.43
33	102	CE	LYS	31	<-->	6083	OE2	GLU	484	3.16
34	102	CE	LYS	31	<-->	6158	OE1	GLN	493	3.7
35	103	NZ	LYS	31	<-->	6081	CD	GLU	484	3.63

36	103	NZ	LYS	31	<-->	6082	OE1	GLU	484	3.66
37	103	NZ	LYS	31	<-->	6083	OE2	GLU	484	2.8
38	103	NZ	LYS	31	<-->	6157	CD	GLN	493	3.86
39	103	NZ	LYS	31	<-->	6158	OE1	GLN	493	2.85
40	127	CB	HIS	34	<-->	5830	OH	TYR	453	3.67
41	128	CG	HIS	34	<-->	5830	OH	TYR	453	3.81
42	129	ND1	HIS	34	<-->	5850	CD1	LEU	455	3.78
43	129	ND1	HIS	34	<-->	5851	CD2	LEU	455	3.57
44	132	CD2	HIS	34	<-->	5830	OH	TYR	453	3.35
45	130	CE1	HIS	34	<-->	5850	CD1	LEU	455	3.49
46	131	NE2	HIS	34	<-->	5850	CD1	LEU	455	3.69
47	139	CD	GLU	35	<-->	6159	NE2	GLN	493	3.69
48	141	OE2	GLU	35	<-->	6157	CD	GLN	493	3.49
49	141	OE2	GLU	35	<-->	6158	OE1	GLN	493	3.33
50	141	OE2	GLU	35	<-->	6159	NE2	GLN	493	2.74
51	154	OE1	GLU	37	<-->	6249	CE2	TYR	505	3.87
52	155	OE2	GLU	37	<-->	6250	CD2	TYR	505	3.76
53	155	OE2	GLU	37	<-->	6249	CE2	TYR	505	3.34
54	161	CG	ASP	38	<-->	5785	CE1	TYR	449	3.71
55	161	CG	ASP	38	<-->	5787	OH	TYR	449	3.37
56	162	OD1	ASP	38	<-->	5785	CE1	TYR	449	3.64
57	162	OD1	ASP	38	<-->	5786	CZ	TYR	449	3.88
58	162	OD1	ASP	38	<-->	5787	OH	TYR	449	3.49
59	162	OD1	ASP	38	<-->	6181	CA	GLY	496	3.53
60	163	OD2	ASP	38	<-->	5785	CE1	TYR	449	3.26
61	163	OD2	ASP	38	<-->	5786	CZ	TYR	449	3.31
62	163	OD2	ASP	38	<-->	5787	OH	TYR	449	2.53
63	189	CD1	TYR	41	<-->	6199	CD	GLN	498	3.77
64	189	CD1	TYR	41	<-->	6200	OE1	GLN	498	3.49
65	190	CE1	TYR	41	<-->	6198	CG	GLN	498	3.88
66	190	CE1	TYR	41	<-->	6199	CD	GLN	498	3.76
67	190	CE1	TYR	41	<-->	6200	OE1	GLN	498	3.53
68	190	CE1	TYR	41	<-->	6222	OD1	ASN	501	3.61
69	193	CE2	TYR	41	<-->	6222	OD1	ASN	501	3.67
70	191	CZ	TYR	41	<-->	6215	OG1	THR	500	3.81
71	191	CZ	TYR	41	<-->	6222	OD1	ASN	501	3.24
72	192	OH	TYR	41	<-->	6216	C	THR	500	3.52
73	192	OH	TYR	41	<-->	6217	O	THR	500	3.6
74	192	OH	TYR	41	<-->	6213	CB	THR	500	3.43
75	192	OH	TYR	41	<-->	6215	OG1	THR	500	2.74
76	192	OH	TYR	41	<-->	6218	N	ASN	501	3.71
77	192	OH	TYR	41	<-->	6222	OD1	ASN	501	3.33

78	201	CD	GLN	42	<-->	5767	O	GLY	446	3.83
79	201	CD	GLN	42	<-->	5787	OH	TYR	449	3.85
80	201	CD	GLN	42	<-->	6201	NE2	GLN	498	3.47
81	202	OE1	GLN	42	<-->	6201	NE2	GLN	498	3.58
82	203	NE2	GLN	42	<-->	5766	C	GLY	446	3.66
83	203	NE2	GLN	42	<-->	5767	O	GLY	446	2.83
84	203	NE2	GLN	42	<-->	5786	CZ	TYR	449	3.73
85	203	NE2	GLN	42	<-->	5787	OH	TYR	449	2.85
86	203	NE2	GLN	42	<-->	6201	NE2	GLN	498	3.05
87	517	CB	MET	82	<-->	6095	CE1	PHE	486	3.52
88	517	CB	MET	82	<-->	6096	CZ	PHE	486	3.67
89	519	SD	MET	82	<-->	6093	CG	PHE	486	3.77
90	519	SD	MET	82	<-->	6094	CD1	PHE	486	3.62
91	519	SD	MET	82	<-->	6095	CE1	PHE	486	3.85
92	528	CE1	TYR	83	<-->	6095	CE1	PHE	486	3.81
93	528	CE1	TYR	83	<-->	6105	OD1	ASN	487	3.6
94	529	CZ	TYR	83	<-->	6095	CE1	PHE	486	3.87
95	529	CZ	TYR	83	<-->	6105	OD1	ASN	487	3.89
96	530	OH	TYR	83	<-->	6094	CD1	PHE	486	3.79
97	530	OH	TYR	83	<-->	6095	CE1	PHE	486	3.7
98	530	OH	TYR	83	<-->	6105	OD1	ASN	487	3.3
99	530	OH	TYR	83	<-->	6122	OH	TYR	489	3.76
100	2551	OD1	ASN	330	<-->	6212	CA	THR	500	3.49
101	2551	OD1	ASN	330	<-->	6217	O	THR	500	3.73
102	2551	OD1	ASN	330	<-->	6213	CB	THR	500	3.23
103	2551	OD1	ASN	330	<-->	6214	CG2	THR	500	3.29
104	2718	CA	LYS	353	<-->	6244	CG	TYR	505	3.52
105	2718	CA	LYS	353	<-->	6245	CD1	TYR	505	3.79
106	2718	CA	LYS	353	<-->	6250	CD2	TYR	505	3.58
107	2724	C	LYS	353	<-->	6243	CB	TYR	505	3.85
108	2724	C	LYS	353	<-->	6244	CG	TYR	505	3.5
109	2724	C	LYS	353	<-->	6245	CD1	TYR	505	3.32
110	2724	C	LYS	353	<-->	6246	CE1	TYR	505	3.79
111	2725	O	LYS	353	<-->	6219	CA	ASN	501	3.64
112	2725	O	LYS	353	<-->	6224	C	ASN	501	3.59
113	2725	O	LYS	353	<-->	6220	CB	ASN	501	3.84
114	2725	O	LYS	353	<-->	6226	N	GLY	502	2.82
115	2725	O	LYS	353	<-->	6227	CA	GLY	502	3.61
116	2725	O	LYS	353	<-->	6229	O	GLY	502	3.63
117	2725	O	LYS	353	<-->	6243	CB	TYR	505	3.36
118	2725	O	LYS	353	<-->	6244	CG	TYR	505	3.47
119	2725	O	LYS	353	<-->	6245	CD1	TYR	505	3.37

120	2719	CB	LYS	353	<-->	6221	CG	ASN	501	3.87
121	2719	CB	LYS	353	<-->	6222	OD1	ASN	501	3.84
122	2719	CB	LYS	353	<-->	6243	CB	TYR	505	3.89
123	2721	CD	LYS	353	<-->	6183	O	GLY	496	3.88
124	2721	CD	LYS	353	<-->	6200	OE1	GLN	498	3.7
125	2721	CD	LYS	353	<-->	6221	CG	ASN	501	3.73
126	2721	CD	LYS	353	<-->	6222	OD1	ASN	501	3.54
127	2721	CD	LYS	353	<-->	6223	ND2	ASN	501	3.52
128	2722	CE	LYS	353	<-->	6183	O	GLY	496	3.8
129	2722	CE	LYS	353	<-->	6200	OE1	GLN	498	3.78
130	2723	NZ	LYS	353	<-->	6181	CA	GLY	496	3.82
131	2723	NZ	LYS	353	<-->	6182	C	GLY	496	3.71
132	2723	NZ	LYS	353	<-->	6183	O	GLY	496	2.84
133	2723	NZ	LYS	353	<-->	6199	CD	GLN	498	3.64
134	2723	NZ	LYS	353	<-->	6200	OE1	GLN	498	2.78
135	2723	NZ	LYS	353	<-->	6201	NE2	GLN	498	3.64
136	2726	N	GLY	354	<-->	6245	CD1	TYR	505	3.65
137	2726	N	GLY	354	<-->	6246	CE1	TYR	505	3.72
138	2728	C	GLY	354	<-->	6226	N	GLY	502	3.64
139	2728	C	GLY	354	<-->	6227	CA	GLY	502	3.7
140	2729	O	GLY	354	<-->	6226	N	GLY	502	3.8
141	2729	O	GLY	354	<-->	6227	CA	GLY	502	3.46
142	2730	N	ASP	355	<-->	6226	N	GLY	502	3.7
143	2732	CB	ASP	355	<-->	6217	O	THR	500	3.38
144	2733	CG	ASP	355	<-->	6217	O	THR	500	3.32
145	2735	OD2	ASP	355	<-->	6217	O	THR	500	3.4
146	2735	OD2	ASP	355	<-->	6213	CB	THR	500	3.85
147	2757	NH2	ARG	357	<-->	6213	CB	THR	500	3.42
148	2757	NH2	ARG	357	<-->	6215	OG1	THR	500	3.65
149	2757	NH2	ARG	357	<-->	6214	CG2	THR	500	3.7

Table 8.8. *List of atom-atom interactions (Salt bridge) across protein-ligand interface in ACE2 (Chain A)-Spike Protein (Chain B) (Delta variant) complex from PDBsum server*

ACE2					Salt bridge	SARS-CoV-2 S protein (Delta)				
Sl.no.	Atom no.	Atom name	Res name	Res no.		Atom no.	Atom name	Res name	Res no.	Distance
1	94	OD2	ASP	30	<-->	5538	NZ	LYS	417	2.68
2	103	NZ	LYS	31	<-->	6082	OE1	GLU	484	2.8

***Table 8.9**. List of atom-atom interactions (Hydrogen bonds) across protein-ligand interface in ACE2 (Chain A)-Spike Protein (Chain B) (Delta-Plus variant) complex from PDBsum server*

ACE2					Hydrogen bonds	SARS-CoV-2 S protein (Delta-Plus)				
Sl.no.	Atom no.	Res name	Res name	Atom no.		Atom no.	Atom name	Res name	Res no.	Distance
1	1	N	SER	19	<-->	11761	O	ALA	475	2.79
2	88	OE1	GLN	24	<-->	11915	ND2	ASN	487	2.52
3	207	NZ	LYS	31	<-->	11876	OE2	GLU	484	2.53
4	207	NZ	LYS	31	<-->	12016	OE1	GLN	493	2.91
5	276	OE2	GLU	35	<-->	12017	NE2	GLN	493	2.79
6	313	OD2	ASP	38	<-->	11288	OH	TYR	449	2.51
7	368	OH	TYR	41	<-->	12122	OG1	THR	500	2.59
8	368	OH	TYR	41	<-->	12122	OG1	THR	500	2.59
9	388	NE2	GLN	42	<-->	11288	OH	TYR	449	2.53
10	4966	ND2	ASN	330	<-->	12125	O	THR	500	3
11	5309	O	LYS	353	<-->	12140	N	GLY	502	3.14
12	5304	NZ	LYS	353	<-->	12060	O	GLY	496	2.49
13	5304	NZ	LYS	353	<-->	12092	OE1	GLN	498	2.87

***Table 8.10**. List of atom-atom interactions (Non-bonded contacts) across protein-ligand interface in ACE2 (Chain A)-Spike Protein (Chain B) (Delta-Plus variant) complex from PDBsum server*

ACE2					Non-bonded contacts	SARS-CoV-2 S protein (Delta-Plus)				
Sl.no.	Atom no.	Atom name	Res name	Res no.		Atom no.	Atom name	Res name	Res no.	Distance
1	1	N	SER	19	<-->	11761	O	ALA	475	2.79
2	81	CB	GLN	24	<-->	11761	O	ALA	475	3.52
3	81	CB	GLN	24	<-->	11914	OD1	ASN	487	3.71
4	84	CG	GLN	24	<-->	11914	OD1	ASN	487	3.71
5	87	CD	GLN	24	<-->	11914	OD1	ASN	487	3.86
6	87	CD	GLN	24	<-->	11915	ND2	ASN	487	3.38
7	88	OE1	GLN	24	<-->	11913	CG	ASN	487	3.31
8	88	OE1	GLN	24	<-->	11914	OD1	ASN	487	3.35
9	88	OE1	GLN	24	<-->	11915	ND2	ASN	487	2.52
10	139	O	THR	27	<-->	11429	CE1	PHE	456	3.78
11	139	O	THR	27	<-->	11431	CZ	PHE	456	3.22
12	130	CB	THR	27	<-->	11756	CB	ALA	475	3.7
13	132	CG2	THR	27	<-->	11429	CE1	PHE	456	3.77
14	132	CG2	THR	27	<-->	11431	CZ	PHE	456	3.76
15	132	CG2	THR	27	<-->	11731	CD2	TYR	473	3.79
16	132	CG2	THR	27	<-->	11729	CE2	TYR	473	3.48
17	132	CG2	THR	27	<-->	11756	CB	ALA	475	3.51
18	132	CG2	THR	27	<-->	11948	CD2	TYR	489	3.8

19	132	CG2	THR	27	<-->	11946	CE2	TYR	489	3.74
20	140	N	PHE	28	<-->	11946	CE2	TYR	489	3.8
21	142	CA	PHE	28	<-->	11946	CE2	TYR	489	3.79
22	142	CA	PHE	28	<-->	11943	CZ	TYR	489	3.86
23	142	CA	PHE	28	<-->	11944	OH	TYR	489	3.5
24	144	CB	PHE	28	<-->	11944	OH	TYR	489	3.14
25	147	CG	PHE	28	<-->	11944	OH	TYR	489	3.61
26	148	CD1	PHE	28	<-->	11944	OH	TYR	489	3.18
27	189	C	ASP	30	<-->	11413	CD2	LEU	455	3.81
28	190	O	ASP	30	<-->	11413	CD2	LEU	455	3.69
29	183	CB	ASP	30	<-->	11429	CE1	PHE	456	3.52
30	183	CB	ASP	30	<-->	11431	CZ	PHE	456	3.74
31	188	OD2	ASP	30	<-->	11407	CG	LEU	455	3.44
32	188	OD2	ASP	30	<-->	11409	CD1	LEU	455	3.12
33	188	OD2	ASP	30	<-->	11413	CD2	LEU	455	3.79
34	188	OD2	ASP	30	<-->	11429	CE1	PHE	456	3.31
35	191	N	LYS	31	<-->	11431	CZ	PHE	456	3.55
36	195	CB	LYS	31	<-->	11938	CG	TYR	489	3.85
37	195	CB	LYS	31	<-->	11948	CD2	TYR	489	3.8
38	198	CG	LYS	31	<-->	11938	CG	TYR	489	3.57
39	198	CG	LYS	31	<-->	11939	CD1	TYR	489	3.55
40	201	CD	LYS	31	<-->	12016	OE1	GLN	493	3.31
41	204	CE	LYS	31	<-->	11874	CD	GLU	484	3.67
42	204	CE	LYS	31	<-->	11875	OE1	GLU	484	3.85
43	204	CE	LYS	31	<-->	11876	OE2	GLU	484	2.77
44	204	CE	LYS	31	<-->	12016	OE1	GLN	493	3.67
45	207	NZ	LYS	31	<-->	11874	CD	GLU	484	3.47
46	207	NZ	LYS	31	<-->	11875	OE1	GLU	484	3.64
47	207	NZ	LYS	31	<-->	11876	OE2	GLU	484	2.53
48	207	NZ	LYS	31	<-->	12016	OE1	GLN	493	2.91
49	251	CB	HIS	34	<-->	11368	OH	TYR	453	3.84
50	254	CG	HIS	34	<-->	11409	CD1	LEU	455	3.78
51	254	CG	HIS	34	<-->	11413	CD2	LEU	455	3.67
52	255	ND1	HIS	34	<-->	11409	CD1	LEU	455	3.62
53	255	ND1	HIS	34	<-->	11413	CD2	LEU	455	3.56
54	260	CD2	HIS	34	<-->	11370	CE2	TYR	453	3.43
55	260	CD2	HIS	34	<-->	11367	CZ	TYR	453	3.81
56	260	CD2	HIS	34	<-->	11368	OH	TYR	453	3.42
57	260	CD2	HIS	34	<-->	11409	CD1	LEU	455	3.43
58	256	CE1	HIS	34	<-->	11409	CD1	LEU	455	3.08
59	256	CE1	HIS	34	<-->	11413	CD2	LEU	455	3.9
60	258	NE2	HIS	34	<-->	11409	CD1	LEU	455	2.95
61	271	CG	GLU	35	<-->	12017	NE2	GLN	493	3.74
62	274	CD	GLU	35	<-->	12017	NE2	GLN	493	3.3

63	276	OE2	GLU	35	<-->	12015	CD	GLN	493	3.49
64	276	OE2	GLU	35	<-->	12016	OE1	GLN	493	3.3
65	276	OE2	GLU	35	<-->	12017	NE2	GLN	493	2.79
66	301	OE2	GLU	37	<-->	12185	CE2	TYR	505	3.67
67	311	CG	ASP	38	<-->	11285	CE1	TYR	449	3.47
68	311	CG	ASP	38	<-->	11287	CZ	TYR	449	3.87
69	311	CG	ASP	38	<-->	11288	OH	TYR	449	3.35
70	312	OD1	ASP	38	<-->	11285	CE1	TYR	449	3.58
71	312	OD1	ASP	38	<-->	11288	OH	TYR	449	3.48
72	312	OD1	ASP	38	<-->	12056	CA	GLY	496	3.27
73	313	OD2	ASP	38	<-->	11285	CE1	TYR	449	2.84
74	313	OD2	ASP	38	<-->	11287	CZ	TYR	449	3.06
75	313	OD2	ASP	38	<-->	11288	OH	TYR	449	2.51
76	372	CD2	TYR	41	<-->	12091	CD	GLN	498	3.55
77	372	CD2	TYR	41	<-->	12092	OE1	GLN	498	3.27
78	365	CE1	TYR	41	<-->	12134	OD1	ASN	501	3.63
79	370	CE2	TYR	41	<-->	12085	CB	GLN	498	3.87
80	370	CE2	TYR	41	<-->	12088	CG	GLN	498	3.67
81	370	CE2	TYR	41	<-->	12091	CD	GLN	498	3.55
82	370	CE2	TYR	41	<-->	12092	OE1	GLN	498	3.33
83	370	CE2	TYR	41	<-->	12134	OD1	ASN	501	3.89
84	367	CZ	TYR	41	<-->	12122	OG1	THR	500	3.69
85	367	CZ	TYR	41	<-->	12134	OD1	ASN	501	3.36
86	368	OH	TYR	41	<-->	12124	C	THR	500	3.46
87	368	OH	TYR	41	<-->	12125	O	THR	500	3.68
88	368	OH	TYR	41	<-->	12116	CB	THR	500	3.27
89	368	OH	TYR	41	<-->	12122	OG1	THR	500	2.59
90	368	OH	TYR	41	<-->	12126	N	ASN	501	3.63
91	368	OH	TYR	41	<-->	12134	OD1	ASN	501	3.41
92	383	CG	GLN	42	<-->	11288	OH	TYR	449	3.48
93	386	CD	GLN	42	<-->	11288	OH	TYR	449	3.4
94	386	CD	GLN	42	<-->	12093	NE2	GLN	498	3.54
95	388	NE2	GLN	42	<-->	11252	C	GLY	446	3.56
96	388	NE2	GLN	42	<-->	11253	O	GLY	446	3.45
97	388	NE2	GLN	42	<-->	11254	N	GLY	447	3.87
98	388	NE2	GLN	42	<-->	11290	CE2	TYR	449	3.68
99	388	NE2	GLN	42	<-->	11287	CZ	TYR	449	3.52
100	388	NE2	GLN	42	<-->	11288	OH	TYR	449	2.53
101	388	NE2	GLN	42	<-->	12093	NE2	GLN	498	3.39
102	428	CD2	LEU	45	<-->	11246	O	VAL	445	3.57
103	1001	O	MET	82	<-->	11898	CZ	PHE	486	3.42
104	989	CB	MET	82	<-->	11894	CD1	PHE	486	3.88
105	989	CB	MET	82	<-->	11896	CE1	PHE	486	3.2
106	989	CB	MET	82	<-->	11898	CZ	PHE	486	3.52

107	995	SD	MET	82	<-->	11894	CD1	PHE	486	3.76
108	1019	CD2	TYR	83	<-->	11898	CZ	PHE	486	3.7
109	1017	CE2	TYR	83	<-->	11896	CE1	PHE	486	3.14
110	1017	CE2	TYR	83	<-->	11898	CZ	PHE	486	3.16
111	1017	CE2	TYR	83	<-->	11914	OD1	ASN	487	3.6
112	1014	CZ	TYR	83	<-->	11896	CE1	PHE	486	3.12
113	1014	CZ	TYR	83	<-->	11898	CZ	PHE	486	3.71
114	1015	OH	TYR	83	<-->	11905	O	PHE	486	3.28
115	1015	OH	TYR	83	<-->	11894	CD1	PHE	486	3.45
116	1015	OH	TYR	83	<-->	11896	CE1	PHE	486	3.09
117	1015	OH	TYR	83	<-->	11914	OD1	ASN	487	3.57
118	1015	OH	TYR	83	<-->	11944	OH	TYR	489	3.27
119	4964	CG	ASN	330	<-->	12118	CG2	THR	500	3.77
120	4965	OD1	ASN	330	<-->	12116	CB	THR	500	3.82
121	4965	OD1	ASN	330	<-->	12118	CG2	THR	500	3.25
122	4966	ND2	ASN	330	<-->	12114	CA	THR	500	3.48
123	4966	ND2	ASN	330	<-->	12124	C	THR	500	3.68
124	4966	ND2	ASN	330	<-->	12125	O	THR	500	3
125	4966	ND2	ASN	330	<-->	12116	CB	THR	500	3.45
126	4966	ND2	ASN	330	<-->	12118	CG2	THR	500	3.8
127	5290	CA	LYS	353	<-->	12174	CB	TYR	505	3.8
128	5290	CA	LYS	353	<-->	12177	CG	TYR	505	3.31
129	5290	CA	LYS	353	<-->	12178	CD1	TYR	505	3.72
130	5290	CA	LYS	353	<-->	12187	CD2	TYR	505	3.32
131	5290	CA	LYS	353	<-->	12185	CE2	TYR	505	3.74
132	5308	C	LYS	353	<-->	12174	CB	TYR	505	3.43
133	5308	C	LYS	353	<-->	12177	CG	TYR	505	3.18
134	5308	C	LYS	353	<-->	12178	CD1	TYR	505	3.22
135	5308	C	LYS	353	<-->	12187	CD2	TYR	505	3.8
136	5309	O	LYS	353	<-->	12128	CA	ASN	501	3.6
137	5309	O	LYS	353	<-->	12138	C	ASN	501	3.82
138	5309	O	LYS	353	<-->	12130	CB	ASN	501	3.43
139	5309	O	LYS	353	<-->	12133	CG	ASN	501	3.87
140	5309	O	LYS	353	<-->	12140	N	GLY	502	3.14
141	5309	O	LYS	353	<-->	12146	O	GLY	502	3.86
142	5309	O	LYS	353	<-->	12174	CB	TYR	505	2.81
143	5309	O	LYS	353	<-->	12177	CG	TYR	505	3.11
144	5309	O	LYS	353	<-->	12178	CD1	TYR	505	3.33
145	5292	CB	LYS	353	<-->	12177	CG	TYR	505	3.88
146	5292	CB	LYS	353	<-->	12187	CD2	TYR	505	3.72
147	5295	CG	LYS	353	<-->	12187	CD2	TYR	505	3.89
148	5301	CE	LYS	353	<-->	12060	O	GLY	496	2.99
149	5301	CE	LYS	353	<-->	12092	OE1	GLN	498	3.69
150	5301	CE	LYS	353	<-->	12135	ND2	ASN	501	3.68

151	5304	NZ	LYS	353	<-->	12056	CA	GLY	496	3.52
152	5304	NZ	LYS	353	<-->	12059	C	GLY	496	3.36
153	5304	NZ	LYS	353	<-->	12060	O	GLY	496	2.49
154	5304	NZ	LYS	353	<-->	12091	CD	GLN	498	3.8
155	5304	NZ	LYS	353	<-->	12092	OE1	GLN	498	2.87
156	5304	NZ	LYS	353	<-->	12093	NE2	GLN	498	3.89
157	5310	N	GLY	354	<-->	12178	CD1	TYR	505	3.45
158	5310	N	GLY	354	<-->	12180	CE1	TYR	505	3.82
159	5312	CA	GLY	354	<-->	12140	N	GLY	502	3.69
160	5312	CA	GLY	354	<-->	12142	CA	GLY	502	3.76
161	5312	CA	GLY	354	<-->	12178	CD1	TYR	505	3.76
162	5315	C	GLY	354	<-->	12140	N	GLY	502	3.14
163	5315	C	GLY	354	<-->	12142	CA	GLY	502	3.3
164	5316	O	GLY	354	<-->	12140	N	GLY	502	3.26
165	5316	O	GLY	354	<-->	12142	CA	GLY	502	2.95
166	5317	N	ASP	355	<-->	12140	N	GLY	502	3.33
167	5319	CA	ASP	355	<-->	12125	O	THR	500	3.9
168	5319	CA	ASP	355	<-->	12140	N	GLY	502	3.86
169	5321	CB	ASP	355	<-->	12125	O	THR	500	3.04
170	5324	CG	ASP	355	<-->	12124	C	THR	500	3.74
171	5324	CG	ASP	355	<-->	12125	O	THR	500	2.79
172	5325	OD1	ASP	355	<-->	12125	O	THR	500	3.2
173	5326	OD2	ASP	355	<-->	12124	C	THR	500	3.66
174	5326	OD2	ASP	355	<-->	12125	O	THR	500	3.06
175	5326	OD2	ASP	355	<-->	12116	CB	THR	500	3.38
176	5326	OD2	ASP	355	<-->	12122	OG1	THR	500	3.75
177	5368	NH2	ARG	357	<-->	12116	CB	THR	500	3.15
178	5368	NH2	ARG	357	<-->	12122	OG1	THR	500	3.61
179	5368	NH2	ARG	357	<-->	12118	CG2	THR	500	3.23

Table 8.11. *List of atom-atom interactions (Salt bridges) across protein-ligand interface in ACE2 (Chain A)-Spike Protein (Chain B) (Delta-Plus variant) complex from PDBsum server*

ACE2						SARS-CoV-2 S protein (Delta-Plus)				
Sl.no.	Atom no.	Atom name	Res name	Res no.	Salt bridges	Atom no.	Atom name	Res name	Res no.	Distance
1	207	NZ	LYS	31	<-->	11876	OE2	GLU	484	2.53

The summarized intermolecular interactions between S protein and ACE2 of the Delta type and mutant complexes at the residue levels were shown in **Figure 8.9.**

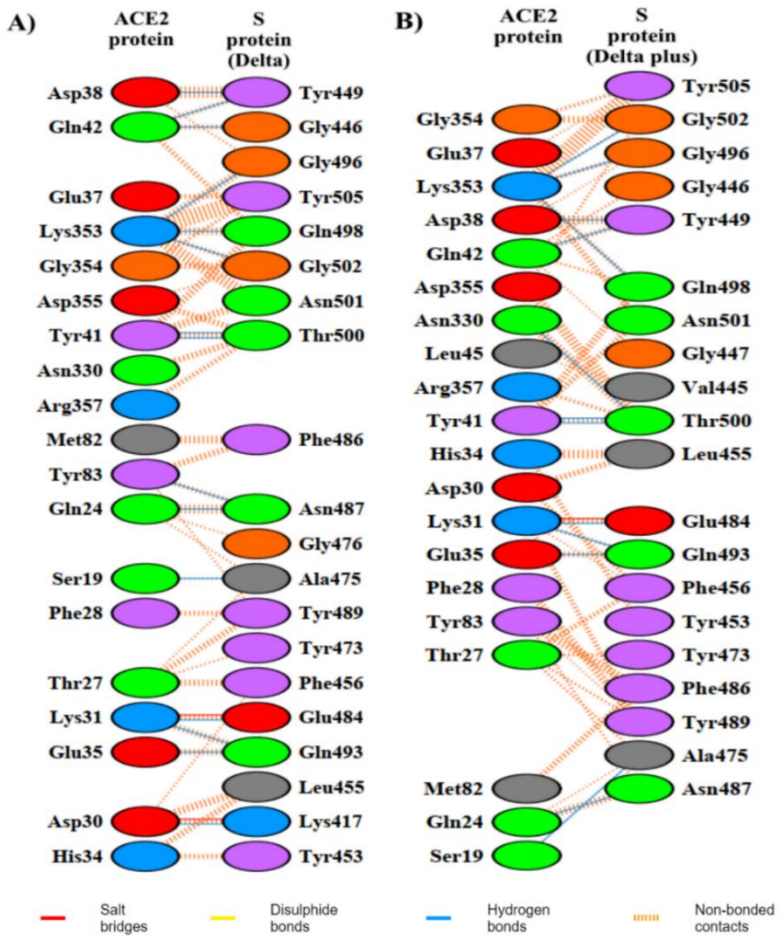

Figure 8.9. *Intermolecular interactions at residue level between ACE2 and S protein in* ***(A)*** *S protein (Delta)-ACE2 and* ***(B)*** *S protein (Delta-Plus)-ACE2 complexes*

8.4.1.5. Binding Free energy and per residue energy decomposition (PRED) analysis.

Binding free energies of the S protein (Delta)-ACE2 and S protein(Delta-Plus)-ACE2 complexes were calculated from the last 10 ns of the MD simulation using MM-PBSA/GBSA approach. The values represent only the relative binding free energy rather than absolute or total binding energy, as MM-PBSA/GBSA approach uses a continuum solvent approach to determine the binding free energies of a system. The binding free energies determined for the Delta and Delta-Plus complexes along with the energy terms, were summarized in **Table 8.12 and 8.13**. From the **Table 8.12 and 8.13**, it can be seen that the S protein(Delta)-ACE2 complex (GB_{TOT} = -39.36 kcal/mol, ΔG_{bind} (GBSA)= -36.08 kcal/mol, PB_{TOT}= -17.52 kcal/mol, ΔG_{bind} (PBSA)= -14.24 kcal/mol) was energetically more favourable than S protein(Delta-Plus)-ACE2 complex (GB_{TOT} = -36.83 kcal/mol, ΔG_{bind} (GBSA)= -33.19 kcal/mol,

PB_{TOT}= -16.03 kcal/mol, ΔG_{bind} (PBSA)= -12.39 kcal/mol). Analysing **Table 8.12 and 8.13**, we observed that all the derived components for the BFE analysis contributed to the binding of S protein and ACE2 to form the S protein (Delta/Delta-Plus)-ACE2 complex.

Table 8.12. *Binding free energies (kcal/mol) and its components of S protein (Delta)-ACE2 and S protein (Delta-Plus)-ACE2 complexes obtained using MM-GBSA approach*

	$\Delta G_{(S\ protein(Delta)-ACE2)} - [\Delta G_{S\ protein(Delta)} + \Delta G_{ACE2}]$ (kcal/mol)		**$\Delta G_{(S\ protein(Delta-Plus)-ACE2)} - [\Delta G_{S\ protein(Delta-Plus)} + \Delta G_{ACE2}]$ (kcal/mol)**	
	Average	**std. dev. (±)**	**Average**	**std. dev. (±)**
VDW	-88.44	4.00	-91.08	4.36
ELE	-1082.33	15.46	-838.42	21.20
GB	1144.23	13.49	906.46	22.31
GBSUR	-12.82	0.34	-13.78	0.40
GAS	-1170.78	15.37	-929.50	22.50
GBSOL	1131.41	13.46	892.67	22.13
GBTOT	-39.36	4.97	-36.83	4.43
TΔS	-3.28	0.22	-3.64	1.44
ΔG_{bind}	**-36.08**		**-33.19**	

Table 8.13. *Binding free energies (kcal/mol) and its components of S protein (Delta)-ACE2 and S protein (Delta-Plus)-ACE2 complexes obtained using MM-PBSA approach*

	$\Delta G_{(S\ protein(Delta)-ACE2)} - [\Delta G_{S\ protein(Delta)} + \Delta G_{ACE2}]$ (kcal/mol)		**$\Delta G_{(S\ protein(Delta-Plus)-ACE2)} - [\Delta G_{S\ protein(Delta-Plus)} + \Delta G_{ACE2}]$ (kcal/mol)**	
	Average	std. dev. (±)	Average	std. dev. (±)
VDW	-88.44	4.00	-91.08	4.36
ELE	-1082.33	15.46	-838.4252	21.2098
PB	1069.90	13.47	847.8183	21.6188
ENPOLAR	-64.76	2.20	-68.5126	1.9070
EDISPER	133.11	2.8868	134.1634	2.2987
GAS	-1170.78	15.3736	-929.5060	22.5022
PBSOL	1168.25	13.6110	913.4691	22.0820
PBTOT	-17.52	7.3209	-16.0368	6.5460
TΔS	-3.28	0.22	-3.64	1.44
ΔG_{bind}	**-14.24**		**-12.39**	

To gain insights into the contribution of the individual amino acid residues to the overall PPI of the S protein (Delta/Delta-Plus)-ACE2 complexes, PRED values were calculated. In this analysis, the total binding energy was decomposed into residues to identify key residues for ACE2 binding to S protein (Delta/Delta-Plus). Essential residues with the binding energy value below -1.00 kcal/mol were shown

in the **Figure 8.10 and 8.11**. The highest energy contributions for S protein (Delta) come from the residues GLN498, GLN493, LYS417, PHE486, TYR505, TYR449, TYR489, PHE456, LEU492, LEU455 and ASN487 while in S protein (Delta-Plus) come from the residues GLY496, ASN487, GLN498, GLN493, TYR505, PHE486, TYR449, TYR489, PHE456, ALA475, LEU492 and LEU455.

(A) MM-GBSA

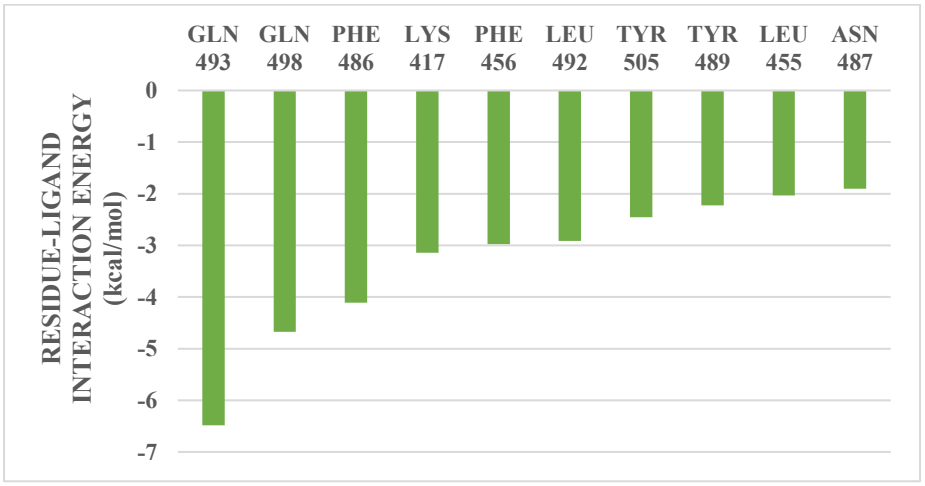

(B) MM-PBSA

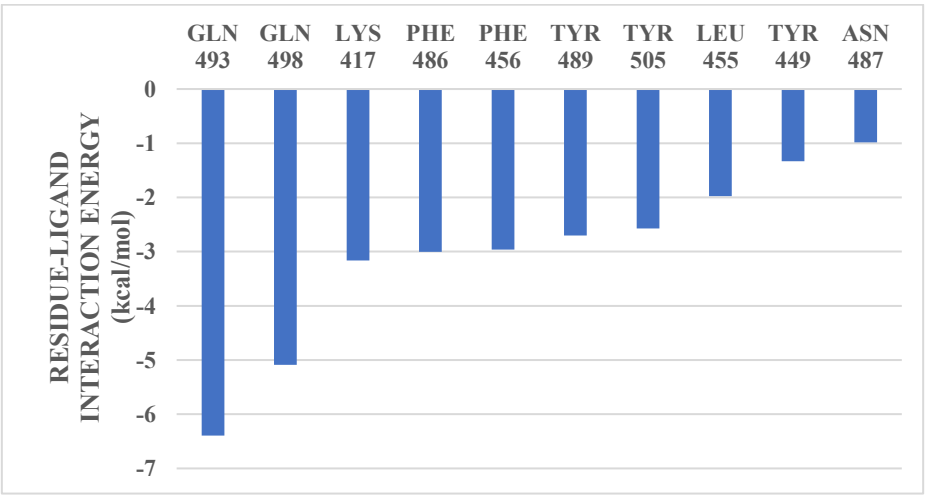

Figure 8.10. *Decomposition of binding free energy (kcal/mol) on per residue basis for ACE2 binding to S protein (Delta) obtained using* ***(A)*** *MM-GBSA approach* ***(B)*** *MM-PBSA approach*

(A) MM-GBSA

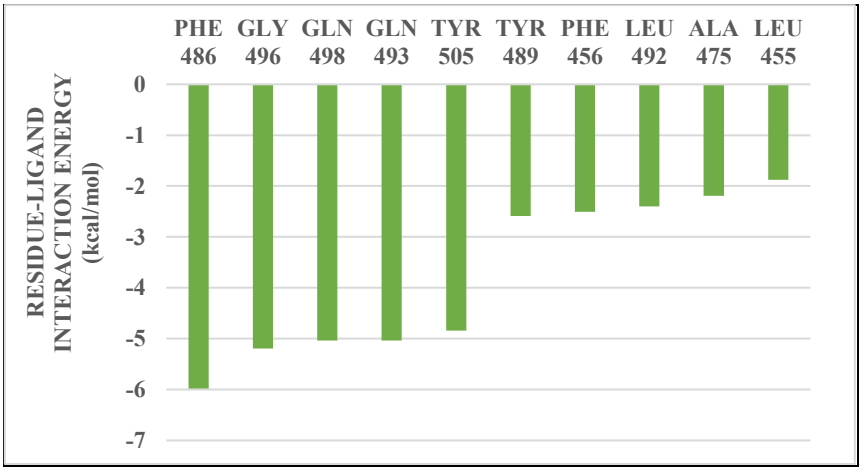

(B) MM-PBSA

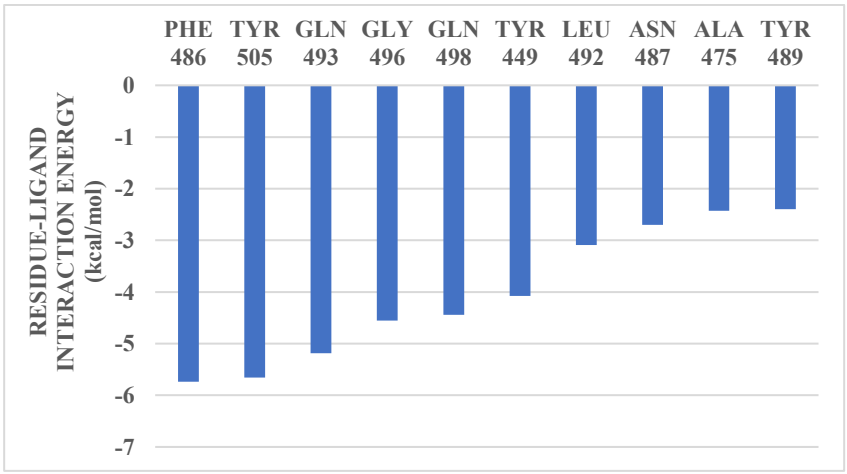

Figure 8.11. *Decomposition of binding free energy (kcal/mol) on per residue basis for ACE2 binding to S protein (Delta-Plus) obtained using* ***(A)*** *MM-GBSA approach* ***(B)*** *MM-PBSA approach*

Discussion: The results section of this chapter provides an insight into the various analyses performed and the coreesponiding results obtained. The Delta-Plus variant (L452R, K417N, and T478K) of the SARS-CoV-2 demonstrates improved structural stability relative to the Delta variant (L452R and T478K) and the wild type. This is evident from the lower RMSD and RMSF values observed for the Delta-Plus complex, especially in the regions surrounding the mutated residues. These findings suggest that the combined effect of the mutations may contribute to a more stable RBD-ACE2 interface.

Further insights into the binding analysis shed light on the fact that the Delta-Plus complex showed more favorable binding energetics when compared to the Delta and wild-type complexes. Notably, the residues located at or near the mutation sites were the major contributors to the total binding energy. These observations indicate that the Delta-Plus variant may possess a stronger and more stable interaction with the ACE2 receptor, potentially contributing to its increased infectivity. The structural and energetic insights gained from those analysis can be valuable for guiding the design of new ligands or therapeutic inhibitors targeting the SARS-CoV-2 spike protein. By identifying key residues particularly around the mutation sites that contribute most significantly to the binding and stability of the spike-ACE2 complex, researchers can focus on these "hotspot" regions to design ligands that can effectively disrupt this interaction.

8.5. Conclusion:

The present study demonstrates the effect of Delta (L452R and T478K) and Delta-Plus (K417N, L452R, and T478K) on the binding of RBD of S protein of SARS-CoV-2 with the ACE2 by employing MD simulation and other computational approaches. From the MD simulation of S protein(Delta)-ACE2 and S protein(Delta-Plus)-ACE2 complexes, we found significant structural changes in the spike protein near the point of mutations (K417N, L452R, and T478K). From the RMSD, RMSF, and PPI analysis, we found S protein(Delta-Plus)-ACE2 complex to have enhanced stability than the S protein(Delta)-ACE2 complex. The binding free energy was found to be subtle higher in the case of the S protein(Delta)-ACE2 than S protein(Delta-Plus)-ACE2 complex. The salient interactions that we have reported in this study pertaining to the S protein and ACE2 in the Delta and the Delta-Plus complexes could be used to design novel inhibitors against the newly emerging coronavirus strains.

8.6. Bibliography:

[1]. Callaway, E. Delta coronavirus variant: scientists brace for impact. *Nature*, *595*(1): 17–18, 2021. https://doi.org/10.1038/d41586-021-01696-3

[2]. Planas, D., Veyer, D., and Baidaliuk, A. Reduced sensitivity of SARS-CoV-2 variant Delta to antibody neutralization. *Nature*, 596(1): 276–280, 2021. https://doi.org/10.1038/s41586-021-03777-9

[3]. Chowdhury, S., and Bappy, M.H. On the Delta Plus Variant of SARS-CoV-2. *European Journal of Medical and Health Sciences*, 3(6): 52–55, 2021. https://doi.org/10.24018/ejmed.2021.3.6.1134

[4]. Bernal, J.L., Andrews, N., Gower, C., Gallagher, E., Simmons, R., Thelwall, S., Stowe, J., Tessier, E., Groves, N., Dabrera, G., Myers, R., Campbell, C., Amirthalingam, G., Edmunds, M., Zambon, M., Brown,

K.E., Hopkins, S., Chand, M., and Ramsay, M. Effectiveness of Covid-19 Vaccines against the B.1.617.2 (Delta) Variant. *The New England Journal of Medicine*, 385(7): 585–594, 2021. http://doi.org/10.1056/NEJMoa2108891

[5]. Salvatore, M., Bhattacharyya, R., Purkayastha, S., Zimmermann, L., Ray, D., Hazra, A., Kleinsasser, M., Mellan, T., Whittaker, C., Flaxman, S., Bhatt, S., Mishra, S., and Mukherjee, B. Resurgence of SARS-CoV-2 in India: Potential Role of the B.1.617.2 (Delta) Variant and Delayed Interventions. *medRxiv*, 2021. https://doi.org/10.1101/2021.06.23.21259405

[6]. Shu, Y., and McCauley, J. GISAID: Global initiative on sharing all influenza data—from vision to reality. *Eurosurveillance*, 22(13), 2017. https://doi.org/10.2807/1560-7917.ES.2017.22.13.30494

[7]. Khateeb, J., Li, Y., and Zhang, H. Emerging SARS-CoV-2 variants of concern and potential intervention approaches. *Critical Care*, 25, 2021. https://doi.org/10.1186/s13054-021-03662-x

[8]. Weisblum, Y. Escape from neutralizing antibodies by sars-cov-2 spike protein variants. *BioRxiv*, 12, 556-561, 2020. https://doi.org/10.1101/2020.07.21.214759

[9]. Verma, J., and Subbarao, N. In-silico study on the effect of SARS-CoV-2 RBD hotspot mutants' interaction with ACE2 to understand the binding affinity and stability. *Virology*, 561, 107–116, 2021. https://doi.org/10.1016/j.virol.2021.06.009

[10]. Teruel, N., Mailhot, O., and Najmanovich, R.J. Modelling conformational state dynamics and its role on infection for Spike protein variants. *PLOS Computational Biology*, 17(6): e1009286, 2021. https://doi.org/10.1371/journal.pcbi.1009286

[11]. Zhang, L., Jackson, C.B., and Mou, H. SARS-CoV-2 spike-protein D614G mutation increases virion spike density and infectivity. *Nature Communications*, 11(1), 2020. https://doi.org/10.1038/s41467-020-19808-4

[12]. Volz, E., Hill, V., and John, T. Evaluating the effects of SARS-CoV-2 spike mutation D614G on transmissibility and pathogenicity. *Cell*, 184: 64–75, 2021. https://doi.org/10.1016/j.cell.2020.11.020

[13]. Noh, J.Y., Jeong, H.W., and Shin, E.C. SARS-CoV-2 mutations, vaccines, and immunity: implication of variants of concern. *Signal Transduction and Targeted Therapy*, 6, 2021. https://doi.org/10.1038/s41392-021-00623-2

[14]. Abdellatiif, MH., Ali, A., Ali, A., and Hussien, M. Computational studies by molecular docking of some antiviral drugs with COVID-19 receptors are an approach to medication for COVID-19. *Open Chemistry*, 19: 245–264, 2021. https://doi.org/10.1515/chem-2021-0024

[15]. Muralidharan, N., Sakthivel, R., Velmurugan, D., and Gromiha, M.M. Computational studies of drug repurposing and synergism of lopinavir, oseltamivir and ritonavir binding with SARS-CoV-2 protease against COVID-19. *Journal of Biomolecular Structure and Dynamics*, 39: 2673–2678, 2021. http://doi.org/10.1080/07391102.2020.1752802

[16]. Mongia, A., Saha, S.K., Chouzenoux, E., and Majumdar, A. A computational approach to aid

clinicians in selecting anti-viral drugs for COVID-19 trials. *Scientific Reports*, 11, 2021. https://doi.org/10.1038/s41598-021 88153-3

[17]. Behera, S.K., Vhora, N., Contractor, D., Shard, A., Kumar, D., Kalia, K., and Jain, A. Computational drug repurposing study elucidating simultaneous inhibition of entry and replication of novel corona virus by Grazoprevir. *Scientific Reports*, 11, 2021. https://doi.org/10.1038/s41598-021-86712-2

[18]. Egieyeh, S., Egieyeh, E., Malan, S., Christofells, A., and Fielding, B. Computational drug repurposing strategy predicted peptide-based drugs that can potentially inhibit the interaction of SARS-CoV-2 spike protein with its target (human ACE2). *PLOS ONE*, 16, 2021. https://doi.org/10.1371/journal.pone.0245258

[19]. Coban, M.A., Morrison, J., Maharjan, S., Hernandez, M.D.H., Li, W., Zhang, Y.S., Freeman, W.D., Radisky, E.S., Le, R.K.G., Weisend, C.M., Ebihara, H., and Caulfield, T.R. Attacking COVID-19 progression using multi-drug for synergetic target engagement. *Biomolecules*, 11, 2021. http://doi.org/10.3390/biom11060787

[20]. Basak, S.C., and Kier, L.B. COVID-19 pandemic: how can computer-assisted methods help to rein in this global menace? *Current Computer-Aided Drug Design*, 17, 2021. http://dx.doi.org/10.2174/1573409917012101121032l5

[21]. Ibrahim, M.A.A., Abdelrahman, A.H.M., Allemailem, K.S., Almatroudi, A., Moustafa, M.F., and Hegazy, M.E.F. In silico evaluation of prospective anti-COVID-19 drug candidates as potential SARS-CoV-2 main protease inhibitors. *The protein journal,* 40(3): 296–309, 2021. https://doi.org/10.1007/s10930-020-09945-6

[22]. Singh, S.K., Upadhyay, A.K., and Reddy, M.S. Screening of potent drug inhibitors against SARS-CoV-2 RNA polymerase: an in-silico approach. *Biotech*, 11: 1–13, 2021. http://doi.org/10.1007/s13205-020-02610-w

[23]. Enmozhi, S.K., Raja, K., Sebastine, I., and Joseph, J. Andrographolide as a potential inhibitor of SARS-CoV-2 main protease: an in-silico approach. *Journal of Biomolecular Structure and Dynamics*, 39(9): 3092–3098, 2021. http://doi.org/10.1080/07391102.2020.1760136

[24]. Mahanta, S., Chowdhury, P., Gogoi, N., Borah, D., Kumar, R., Chetia, D., Borah, P., Buragohain, A.K., and Gogoi, B. Potential anti-viral activity of approved repurposed drug against main protease of SARS-CoV-2: an in-silico based approach. *Journal of Biomolecular Structure and Dynamics*, 39(10): 3802–3811, 2021. http://doi.org/10.1080/07391102.2020.1768902

[25]. Beura, S., and Chetti, P. In-silico strategies for probing chloroquine-based inhibitors against SARS-CoV-2. *Journal of Biomolecular Structure and Dynamics*, 39(10): 3747–3759, 2021. http://doi.org/10.1080/07391102.2020.1772111

[26]. Mittal, L., Kumari, A., Srivastava, M., Singh, M., and Asthana, S. Identification of potential molecules against COVID-19 main protease through structure-guided virtual screening approach. *Journal of Biomolecular Structure and Dynamics*, 39(10): 3662–3680, 2021.

http://doi.org/10.1080/07391102.2020.1768151

[27]. Wahedi, H.M., Ahmad, S., and Abbasi, S.W. Stilbene-based natural compounds as promising drug candidates against SARS-CoV-2. *Journal of Biomolecular Structure and Dynamics*, 39: 3225–3234, 2021. http://doi.org/10.1080/07391102.2020.1762743

[28]. Selvaraj, C., Dinesh, D.C., Panwar, U., Abhirami, R., Boura, E., and Singh, S.K. Structure-based virtual screening and molecular dynamics simulation of SARS-CoV-2 guanine-N7 methyltransferase (nsp14) for identifying antiviral inhibitors against COVID-19. *Journal of Biomolecular Structure and Dynamics*, 39(13): 4582–4593, 2021. http://doi.org/10.1080/07391102.2020.1778535

[29]. Hassab, M.A.E., Ibrahim, T.M., Al-Rashood, S.T., Alharbi, A., Eskandrani, R.O., and Eldehna, W.M. In silico identification of novel SARS-COV-2 2-O-methyltransferase (nsp16) inhibitors: structure-based virtual screening, molecular dynamics simulation and MM-PBSA approaches. *Journal of Enzyme Inhibition and Medicinal Chemistry*, 36(1): 727–736, 2021. http://doi.org/10.1080/14756366.2021.1885396

[30]. Elmaaty, A.A., Darwish, K.M., Khattab, M., Elhady, S.S., Salah, M., Hamed, M.I. A., Al-Karmalawy, A.A., and Saleh, M.M. In a search for potential drug candidates for combating COVID-19: computational study revealed salvianolic acid B as a potential therapeutic targeting 3CLpro and spike proteins. *Journal of Biomolecular Structure and Dynamics*, 40(19): 8866–8893, 2022. https://doi.org/10.1080/07391102.2021.1918256

[31]. Al-Karmalawy, A., Alnajjar, R., Dahab, M., Metwaly, A., and Eissa, I.H. Molecular docking and dynamics simulations reveal the potential of anti-HCV drugs to inhibit COVID-19 main protease. *Pharmaceutical Sciences*, 27: S109-S121, 2021. https://doi.org/10.34172/PS.2021.3

[32]. Sharanya, C.S., Sabu, A., and Haridas, M. Potent phytochemicals against COVID-19 infection from phyto materials used as antivirals in complementary medicines: a review. *Future Journal of Pharmaceutical Sciences*, 7, 2021. https://doi.org/10.1186/s43094-021-00259-7

[33]. Nabi, F., Ahmad, O., Khan, Y.A., Nabi, A., Amiruddin, H.M., Qais, F.A., Masroor, A., Hisamuddin, M., Uversky, V.N., and Khan, R.H. Computational studies on phylogeny and drug designing using molecular simulations for COVID-19. *Journal of Biomolecular Structure and Dynamics*, 40(21): 10753–10762, 2021. http://doi.org/10.1080/07391102.2021.1947895

[34]. Berman, H. M., Westbrook, J., Feng, Z., Gilliland, G., Bhat, T. N., Weissig, H., Shindyalov, I. N., and Bourne, P. E. The Protein Data Bank. *Nucleic Acids Research,* 28(1): 235–242, 2000. https://doi.org/10.1093/nar/28.1.235

[35]. Pettersen, E. F., Goddard, T. D., Huang, C. C., Couch, G. S., Greenblatt, D. M., Meng, E. C., and Ferrin, T. E. UCSF Chimera—A visualization system for exploratory research and analysis. *Journal of Computational Chemistry,* 25(13): 1605–1612, 2004. https://doi.org/10.1002/jcc.20084

[36]. Salomon-Ferrer, R., Götz, A. W., Poole, D., Le Grand, S., and Walker, R. C. Routine microsecond

molecular dynamics simulations with AMBER on GPUs. 2. Explicit solvent particle mesh Ewald. *Journal of Chemical Theory and Computation,* 9(9): 3878–3888, 2013. https://doi.org/10.1021/ct400314y

[37]. Jorgensen, W. L., Chandrasekhar, J., Madura, J. D., Impey, R. W., and Klein, M. L. Comparison of simple potential functions for simulating liquid water. *The Journal of Chemical Physics*, 79(2): 926–935, 1983. https://doi.org/10.1063/1.445869

[38]. Darden, T., York, D., and Pedersen, L. Particle mesh Ewald: An N·log(N) method for Ewald sums in large systems. *The Journal of Chemical Physics*, 98(12): 10089–10092, 1993. https://doi.org/10.1063/1.464397

[39]. Ryckaert, J.-P., Ciccotti, G., and Berendsen, H. J. C. Numerical integration of the Cartesian equations of motion of a system with constraints: Molecular dynamics of *n*-alkanes. *Journal of Computational Physics,* 23(3): 327–341, 1977. https://doi.org/10.1016/0021-9991(77)90098-5

[40]. Berendsen, H. J., Postma, J. V., van Gunsteren, W. F., DiNola, A., and Haak, J. R. Molecular dynamics with coupling to an external bath. *The Journal of Chemical Physics,* 81(8): 3684–3690, 1984. https://doi.org/10.1063/1.448118

[41]. Krautler V, Gunsteren W.F.V., and Hunenberger P.H. A fast SHAKE: Algorithm to solve distance constraint equations for small molecules in molecular dynamics simulations. *Journal of Computational Chemistry,* 22: 501-508, 2001. http://dx.doi.org/10.1002/1096-987X(20010415)22:53.0.CO;2-V

[42]. Laskowski, R. A., Hutchinson, E. G., Michie, A. D., Wallace, A. C., Jones, M. L., and Thornton, J. M. PDBsum: A web-based database of summaries and analyses of all PDB structures. *Trends in Biochemical Sciences,* 22(12): 488–490, 1997. https://doi.org/10.1016/s0968-0004(97)01140-7

[43]. Chen, F., Liu, H., Sun, H., Pan, P., Li, Y., Li, D., and Hou, T. Assessing the performance of the MM/PBSA and MM/GBSA methods. 6. Capability to predict protein–protein binding free energies and re-rank binding poses generated by protein–protein docking. *Physical Chemistry Chemical Physics,* 18(30): 22129–22139, 2016. https://doi.org/10.1261/rna.065896.118

[44]. Genheden, S., and Ryde, U. The MM/PBSA and MM/GBSA methods to estimate ligand-binding affinities. *Expert Opinion on Drug Discovery, 10*(5): 449–461, 2015. https://doi.org/10.1517/17460441.2015.1032936

[45]. Sun, H., Duan, L., Chen, F., Liu, H., Wang, Z., Pan, P., Zhu, F., Zhang, J. Z. H., and Hou, T. Assessing the performance of MM/PBSA and MM/GBSA methods. 7. Entropy effects on the performance of end-point binding free energy calculation approaches. *Physical Chemistry Chemical Physics,* 20(22): 14450–14460, 2018. https://doi.org/10.1039/c7cp07623a

[46]. Wang, E., Sun, H., Wang, J., Wang, Z., Liu, H., Zhang, J. Z. H., and Hou, T. End-point binding free energy calculation with MM/PBSA and MM/GBSA: Strategies and applications in drug design. *Chemical Reviews,* 119(16): 9478–9508, 2019. https://doi.org/10.1021/acs.chemrev.9b00055

[47]. Case, D. A. Normal mode analysis of protein dynamics. *Current Opinion in Structural Biology,* 4(2): 285–290, 1994. https://doi.org/10.1016/S0959-440X(94)90321-2

[48]. Chen, J., Yin, B., Pang, L., Wang, W., Zhang, J.Z., and Zhu, T. Binding modes and conformational changes of FK506-binding protein 51 induced by inhibitor bindings: insight into molecular mechanisms based on multiple simulation technologies. *Journal of Biomolecular Structure and Dynamics*, 38: 1–15, 2019. http://doi.org/10.1021/acs.jcim.0c01470

[49]. Du, Q., Qian, Y., Yao, X., and Xue, W. Elucidating the tight-binding mechanism of two oral anticoagulants to factor Xa by using induced-fit docking and molecular dynamics simulation. *Journal of Biomolecular Structure and Dynamics*, 38(2): 625–633, 2019. https://doi.org/10.1080/07391102.2019.1583605

[50]. Eduardo, S.C.E., Betancourt-Conde, I., Hernandez-Campos, A., Tellez-Valencia, A., and Castillo, R. In silico hit optimization toward AKT inhibition: fragment-based approach, molecular docking and molecular dynamics study. *Journal of Biomolecular Structure and Dynamics*, 37: 4301–4311, 2019. http://doi.org/10.1080/07391102.2018.1546618

[51]. Gao, J., Wang, Y., Chen, Q., and Yao, R. Integrating molecular dynamics simulation and molecular mechanics/generalized Born surface area calculation into pharmacophore modeling: a case study on the proviral integration site for Moloney murine leukemia virus (Pim)-1 kinase inhibitors. *Journal of Biomolecular Structure and Dynamics*, 38(2): 581–588, 2019. http://doi.org/10.1080/07391102.2019.1571946

[52]. Joshi, T., Joshi, T., Sharma, P., Chandra, S., and Pande, V. Molecular docking and molecular dynamics simulation approach to screen natural compounds for inhibition of Xanthomonas oryzae pv. Oryzae by targeting Peptide Deformylase. *Journal of Biomolecular Structure and Dynamics*, 39: 1–40, 2020. https://doi.org/10.1080/07391102.2020.1719200

[53]. Sk, M.F., Roy, R., and Kar, P. Exploring the potency of currently used drugs against HIV-1 protease of subtype D variant by using multiscale simulations. *Journal of Biomolecular Structure and Dynamics*, 39(3): 988–1003, 2020. https://doi.org/10.1080/07391102.2020.1724196

[54]. Wan, Y., Guan, S., Qian, M., Huang, H., Han, F., Wang, S., and Zhang, H. Structural basis of fullerene derivatives as novel potent inhibitors of protein acetylcholinesterase without catalytic active site interaction: insight into the inhibitory mechanism through molecular modeling studies. *Journal of Biomolecular Structure and Dynamics*, 38(2): 410-425, 2020. https://doi.org/10.1080/07391102.2019.1576543

[55]. Zhang, W., Yang, F., Ou, D., Lin, G., Huang, A., Liu, N., and Li, P. Prediction, docking study, and molecular simulation of 3D DNA aptamers to their targets of endocrine-disrupting chemicals. *Journal of Biomolecular Structure and Dynamics,* 37(16): 4274–4282, 2019. https://doi.org/10.1080/07391102.2018.1547222